UNIVERSITY OF OKLAHOMA

GRADUATE COLLEGE

INVESTIGATION OF DRILLSTRING VIBRATIONS USING FINITE ELEMENT METHOD SIMULATIONS AND DESIGN AND IMPLEMENTATION OF EXPERIMENTAL SETUP

A THESIS

SUBMITTED TO THE GRADUATE FACULTY

in partial fulfillment of the requirements for the

Degree of

MASTER OF SCIENCE

By

ANTONIO RAFAEL MARQUEZ CHACIN
Norman, Oklahoma
2017

INVESTIGATION OF DRILLSTRING VIBRATIONS USING FINITE ELEMENT METHOD SIMULATIONS AND DESIGN AND IMPLEMENTATION OF EXPERIMENTAL SETUP

A THESIS APPROVED FOR THE
MEWBOURNE SCHOOL OF PETROLEUM AND GEOLOGICAL ENGINEERING

BY

_____
Dr. Catalin Teodoriu, Chair

_____
Dr. Ramadan Ahmed

_____
Dr. James D. Baldwin

This work is dedicated to my late mother Maritza Chacin and to my wife Jodi Marquez whose unconditional love and support have made me the man I am today.

Acknowledgements

First and foremost, I would like to thank PD Dr. Dr.-ing. Habil Catalin Teodoriu for his continued support, guidance and mentoring throughout the length of the project and my studies. Without him this investigation would not have been possible. To Dr. James Baldwin for igniting my interest in the field of mechanical vibrations and challenging me to think critically during the first downscaled vibration setup that I build with his help.

To Billy and Greg from the Mechanical Engineering department machine shop. For not only helping me make or fix some of the parts I made for this project but also for their teachings and good conversations during the past two years.

To the support, love and teachings of my late mother Maritza Chacin. Without her, nothing that I have accomplished up to this point would have been possible.

To the continuous and unconditional support of my wife Jodi Marquez that has motivated me to be better and work harder every day.

To my father, family, Zena Amer and extended family through my wife, for their help, encouragement, support, motivation and advice.

I would also like to thank ConocoPhillips for sponsoring the necessary funds to purchase the equipment necessary for the successful completion of this project.

To my friends and people who have directly or indirectly have supported me for me to accomplish my goals.

To all, my deepest and sincerest appreciation.

Antonio R. Marquez Chacin

Table of Contents

List of Tables

List of Figures

Abstract

In this study, an extensive assortment of the principal studies related to drill-string vibrations is presented, focusing on analytical studies, finite element models and experimental setups. A discussion on the current limitations of the current experimental research is discussed and is used to design a new experimental setup that will cover most of those limitations. Two finite different studies are presented. The first study compares six different cases to a simplified bottom-hole-assembly and concludes that when all three modes of vibration are induced in the system, the vibration response will be lower than when a single mode of vibration is applied. The second study extended the scope of the previous study and modelled the behavior of the downscaled geometry proposed for the experimental setup, comparing four different materials when one mode of vibration is induced versus all modes of vibration. The results are compared graphically and numerically using the damping ratio and response frequency. Additionally, a modal analysis comparing the first 140 modes of natural frequencies is presented for the four studied materials. It was concluded that, similarly to the previous study, the vibration response is lower when all modes of vibration are applied than when only one mode is induced. It was concluded as well from this study that when one mode of vibration is applied, the behavior of the vibration response is predictable according to known analytical models, but when all modes are present in the system, the behavior will vary considerably. Finally, a in detail description of a designed and build experimental setup is presented and the future steps are described in order to ultimately mitigate downhole vibrations in a safe, cost effective and environmentally responsible manner.

Chapter 1: Introduction

1.1 Motivation

In the oil and gas industry the ultimate objective is to achieve the successful retrieval of hydrocarbons from the reservoir in a safe, cost effective, and environmental friendly manner. The most critical process in order to achieve this objective comes with the drilling process of the well. The drilling process in turn, represents the biggest portion of the cost of the development of a well, due to the high level of intricacies, unknown parameters and risk management. Therefore, this process needs to be planned, monitored and executed in a safe and efficient manner.

The drilling process consist of the mechanical energy transfer from the top to the drilling bit with the rotation of the drilling pipe by the rotary system. The rotary system applies the torque to rotate the entire string and drilling bit. The necessary weight-on-bit (WOB) is controlled by the hoisting system. Finally, the lifting of the rock cuttings is made by the circulating system.

The optimization and effectiveness of the drilling process is dependent upon many factors such as the technology available at the drilling location, the drilling crew, the geological formation to be drilled, the depth of the target reservoir, the direction at which the target needs to be reach, among many others. One of the most critical factors to consider is drill-string dynamics.

Undesired drill-string vibrations may cause not only a reduction of rate of penetration (ROP), but also bottom hole assembly (BHA) tool failure or excessive wear (Kapitaniak, et al. 2015, 324-337) (Younggang, et al. 2011) (Moradi and Ranjbar 2009, 923-933).

1.2 Problem Description

There are three modes of vibrations which affects the drill-string during operation: torsional, lateral and axial (Sotomayor, Placido and Cunha 1997) (Patil and Teodoriu 2013, 227-238). In the industry, each one of these modes generate a specific drilling problem. The axial vibrations generate a repeated separation between the bottom hole and the drilling-bit, this problem is known as “bit bouncing”. The lateral movements of the drill-string that causes repeated shocks between the bore-hole and the drill-pipe is called “whirling”. Finally, the most common, and often most detrimental, type of drilling problem called “stick-slip” it’s associated with vibrations due to the torsional vibrations in the drill-string. (Tucker and Wang 1999, 123-165) (Omojuwa, Osisanya and Ahmed, Measuring and Controlling Torsional Vibrations and Stick-Slip in a viscous-Damped Drillstring Model 2011).

Bit bouncing is generally observed in vertical to near vertical wells, when using tricone bits, when drilling out the shoe track (i.e. full-sized length of casing placed at the bottom of the casing string that is usually left full of cement on the inside to ensure that good cement remains on the outside of the bottom of the casing), and in hard formations or stringers. It may also be generated by the combined effect of other vibration problems such as whirling and stick-slip. Some signs of bit bouncing at the surface include: shaking of the top drive or kelly and WOB fluctuation. Some measures that have been used to mitigate this issue include the reduction of WOB and the increasing of RPM, changing the bit design as well as the option to include a shock sub in the BHA (Ashley, McNary and Tomlinson 2001).

Whirling occurs when the Bit and/or the BHA rotates eccentrically around the wellbore instead of its rotating center. The bit whirls due to its interaction with the formation. It is generally observed when transitioning between a soft and hard formation and near-vertical wells. The BHA whirling is a more complex in its inducing conditions but it is considerably more detrimental for the drilling operations. It will mainly occur when the BHA doesn't have any type of stabilizers and the well is near vertical but, other conditions such as bad lubricity of the well and washout boreholes considerably affect the severity of these vibrations. (Ashley, McNary and Tomlinson 2001).

Although these are both a consequence of the same mode of vibration, they are both diagnosed and treated differently. Bit whirling is difficult to recognize at the surface unless it is severe. However, this problem may cause premature BHA failure, bit failure and reduce significantly ROP. BHA whirling can be recognize at the surface because it usually induces other types of vibration problems such as bit bouncing. Both of these problems are usually recognized using specialized downhole tools such as Measure-While-Drilling (MWD). They can be mitigated by stopping momentarily drilling operations or reducing WOB and increasing RPM. (Ashley, McNary and Tomlinson 2001)

Stick-slip is a drilling dysfunction that is characterized by large oscillations of the bit rpm (Pavone and Desplans 1994). The bit will stop periodically causing the string to torque up and when the torque is sufficiently high it will spin free back and forward until it reaches an equilibrium point or it continues its vibration. It is generally observed in "high angle wells, when aggressive PDC bits are used and in environments where the BHA to wellbore friction is high" (Ashley, McNary and Tomlinson 2001). The phenomena can

be detected at surface by the presence of a ratty surface torque and fluctuating RPM. Some of the consequences of leaving this problem untreated is the over torque and damaged connections that could lead to washouts, the removal of cutters from PDC bits and teeth from roller cone bits. Among the general practice mechanisms to deal with this issue is the reduction of WOB and RPM, reduction of friction by using roller reamers or increasing the mud lubricity, and having a smooth well profile (Ashley, McNary and Tomlinson 2001).

All of these drilling vibrations are always present in drilling operations but they only become a problem when the oscillations in any axis (lateral, axial and torsional) come close to the natural frequencies of the system, thus reaching resonance. A summary of the frequencies at which these vibrations become an observable problem is presented by Esmaeili et al (2012) from field measurements presented in Macpherson et al (1993). The frequency ranges are shown in **Figure 1**.

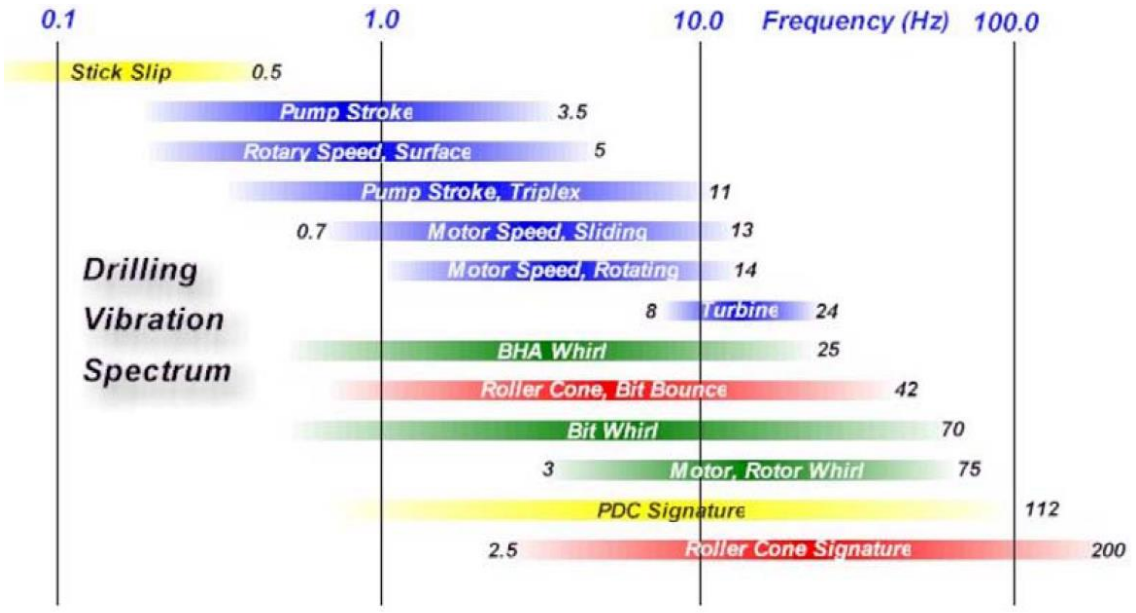

Figure 1. Drilling vibration spectrum of frequency ranges by Esmaeili et al (2012)

1.3 Mechanical Vibrations Introduction

Mechanical vibrations can be defined as "…periodic exchange of potential and kinetic energy". The main components of any mechanical system (such as a drill-string) are its mass and stiffness. Additionally, the system will have inherently some damping associated with it. The mass component relates the system's forces and acceleration (Newton's 2nd law). The motion of this mass it's what generates the potential energy of the system. The stiffness component relates the system's forces and displacement (Hook's law). The displacement of the stiffness component generates kinetic energy. Finally, the damping component will be responsible for the energy dissipation. Whatever the source of the damping of the system is, it will convert kinetic and potential energy into heat, which is lost. (Schmitz and Smith 2011)

There are three general categories for mechanical vibrations: free vibrations, forced vibrations and self-excited vibrations.

Free Vibrations occur when a system is initially at rest and in a stable equilibrium condition, then it is disturbed with a force out of its equilibrium position. The system will vibrate until it reaches its initial equilibrium condition again. An example of free vibration's behavior is shown in **Figure 2**. As it can be seen, free vibration is observed as an exponentially decaying, periodic response to the initial disturbance (Schmitz and Smith 2011).

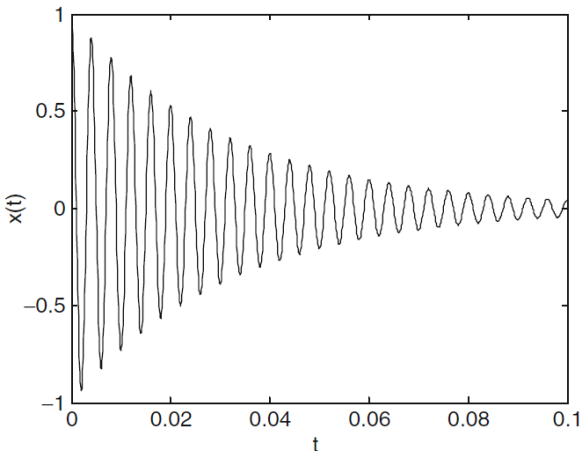

Figure 2. Free vibration example. (Schmitz and Smith, 2011)

Forced Vibration occur when instead of a single disturbance to the system, a continuing periodic excitation is applied. When initially applied, the system will experience a transient state behavior to then reach a steady state in which the system response will be similar to the disturbance function and the system's vibrating frequency matches the forcing frequency. It is important to note that, once the recurring disturbance stops, the system then becomes a free vibrating system in which it will return to its original equilibrium position. Forced vibration is usually represented in a magnitude vs. frequency domain as shown in **Figure 3**. (Schmitz and Smith 2011)

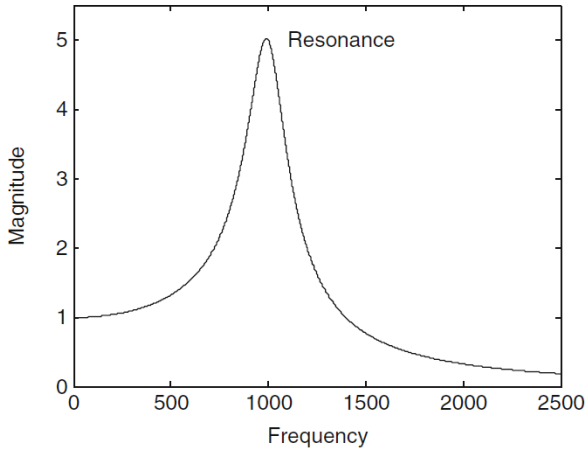

Figure 3. Forced vibration example. (Schmitz and Smith, 2011)

When the forcing frequency is equal to the system's natural frequency, this is known as *resonance.* This is identified where the forcing or disturbance's frequency is equal to the natural frequency. (Schmitz and Smith 2011)

Self-Excited Vibration occurs when "a steady input force is modulated into vibrations near the system's natural system". Unlike free vibration, the disturbance is long lasting and unlike forced vibration, the disturbance is steady rather than periodic and revolves around its natural frequency. A good example given by Schmitz and Smith (2011) is the sound that a bow and a string make in a violin. The friction between the string and the bow generate vibrations that make different sounds depending on the speed at which the bow moves across the string. A representation of the behavior observed with self-excited vibration is shown in **Figure 4**. (Schmitz and Smith 2011)

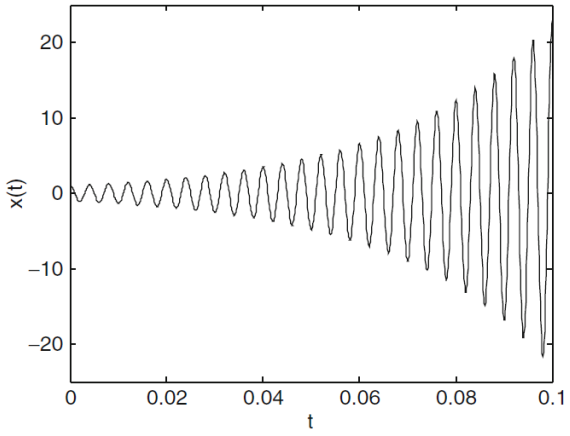

Figure 4. Self-excited vibration. (Schmitz and Smith, 2011)

1.3.1 Dampening of harmonic systems

There are three types of damping that are used for physical models:

Viscous Damping relates the resistance on a body that is moving through a fluid at a certain velocity. It is one of the prefer damping methods due to its mathematical simplicity. Even if the problem at hand does not involve a viscous fluid, an equivalent viscous damping can be found by obtaining the damping ratio from experimental or simulation data. If the vibration response is obtained, the damping ratio can be found by calculating the natural logarithm of two peak values (represented as x1 and x2 in **Figure 5**), and then divide this quantity by 2π (Schmitz and Smith 2011). If the two selected peaks are not consecutive, this value is also divided by the number of cycles between the peaks yielding the following expression,

$$\xi_{equivalent} = \frac{\ln\left(\frac{X_1}{X_2}\right)}{2\pi N}$$

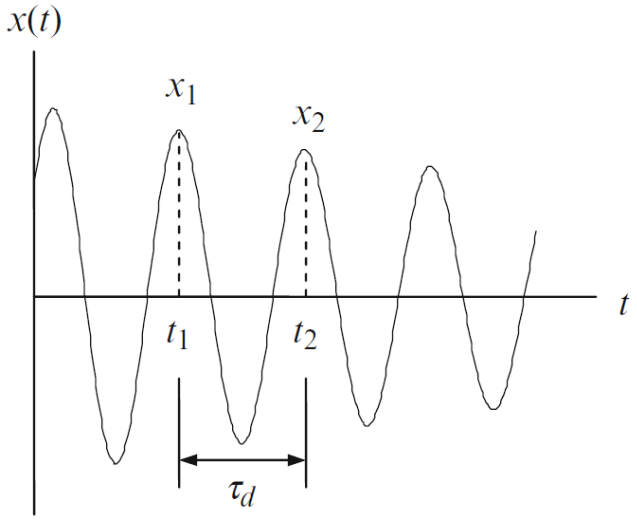

Figure 5. Vibration Spectrum Response. (Schmitz and Smith 2011)

Coulomb Damping represents the energy dissipation due to the frictional interaction between two dry surfaces (Schmitz and Smith 2011). For the purposes of this research, this type of dampening will not be considered as it escapes the scope and objective of this study.

Finally, *Solid Damping* occurs due to the dissipation of internal energy in a vibrating solid (Schmitz and Smith 2011). Every solid body will have the tendency to damp any vibration that it's affecting it.

1.3.2. Rayleigh Damping

Rayleigh Damping is a useful tool that is used to deal with multi degrees of freedom systems and consider the system to have an equivalent viscous damping even if there is no fluid in the system. The viscous damping assumption is that damping is directly proportional to the velocity, which can be described by Rayleigh dissipation function as described by the following expression (Liu and Gorman 1994),

$$R(t) = \frac{1}{2}\iiint_V \mu\, \dot{u}^2(x,y,z,t)dv + \frac{1}{2}\sum C_i \dot{u}^2(x,y,z,t)$$

"Where μ is an energy dissipation coefficient, C are discrete damping factors and u(x,y,z,t) is a displacement function for which the normal finite element discretization is available which produces a set of discretized second-order differential equations derived by using the variational principle" (Liu and Gorman 1994).

Then, the equation of motion of a linear dynamic system can be written as,

$$[M]\{\ddot{x}\} + [C]\{\dot{x}\} + [K]\{x\} = \{f\}$$

Where [M], [C] and [K] are the mass, damping and stiffness matrices and {x} and {f} are displacement and force vectors respectively.

Due to the difficulty and intricacies of obtaining a system's damping, a common expression of the Rayleigh damping for small levels of damping is given by the following expression (Liu and Gorman 1994),

$$[C] = [M]\sum_{k=0}^{p\sim 1} \sigma_k \left([M]^{-1}[K]\right)^k$$

The simples form of this expression however is the case for proportional damping consisting of only two terms as follows,

$$[C] = \alpha_0[M] + \alpha_1[K]$$

Where α_0 and α_1 are arbitrary constant coefficients (Liu and Gorman 1994).

In the software Ansys Workbench V 17.1, used in this thesis extensively, these constants are described as the usual Alpha and Beta letters from the Greek alphabet. In the help section of the software where it describes the Rayleigh Damping in detail, it explains that these "values are not generally known directly, but are calculated from modal damping ratios…". The expression given to find this relation is as follows,

$$\xi_i = \frac{\alpha}{2\omega_i} + \frac{\beta\omega_i}{2}$$

Where, ξ_i is the ratio of actual damping to critical damping for a particular mode of vibration, i. and ω_i is the natural circular frequency of mode i. The manual, goes further to explain "to explain both α and β for a given damping ratio ξ_i, it is commonly assumed that the sum of α and β terms is nearly constant over a range of frequencies. Therefore, given ξ and a frequency range ω_1 to ω_2 two simultaneous equations can be solved for α and β. These expressions are presented as follows,

$$\alpha = 2\xi\frac{\omega_1\omega_2}{\omega_1 + \omega_2}$$

$$\beta = \frac{2\xi}{\omega_1 + \omega_2}$$

This is derived from the graphical representation shown in **Figure 6**.

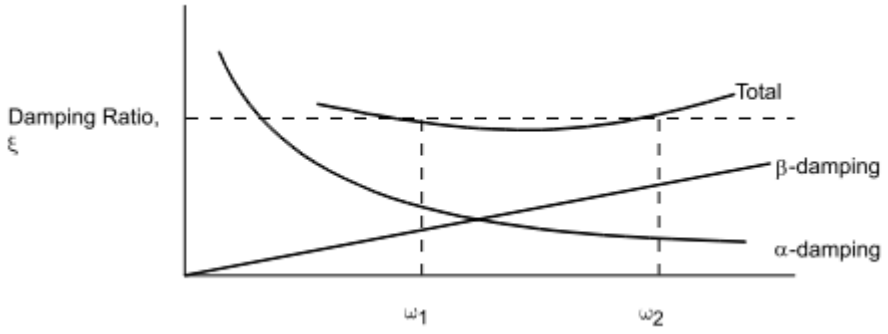

Figure 6. Alpha and Beta Damping Relationship (Reyleigh Damping).

An important warning and further explanation is given in the manual of the use of this type of damping for Finite Element Analysis. It explains that the use of alpha damping can lead to "undesirable results if an artificially large mas has been introduced into the model". And if the use of Beta damping can lead to "undesirable results in a nonlinear analysis" because these coefficients are multiplied by the stiffness matrix which is constantly changing in a nonlinear analysis.

Given the complexity and significant impact that the selection of these coefficient has on a nonlinear analysis, it is highly recommended that these are derived from experimental data instead of a "trial and error" approach. To find these values experimentally, the damping ratio vs natural frequencies relation should be found with the experimental setup already completed.

Chapter 2: Current Research

Research related to drill-string dynamics it is not new. In the 1960s it began a wave of research trying to accurately describe and understand the drill-string dynamics with the purpose of optimizing the drilling process and brining the cost down (Darein and Livesay 1968) (Shor, Pryor and Oort 2014). These models have increased in complexity with time and with the advancement of computational resources and power (Darein and Livesay 1968) (Leine, Campen and Keultjes April, 2002).

2.1 Analytical Modelling

Analytical models have been divided into mainly two categories: Soft-string and stiff-string models. *Soft-string* model is a lumped mass model that assumes continuous drillstring-borehole contact while a *stiff-string* explicitly calculates bending and may assume contacts with the borehole (Darein and Livesay 1968).

The simplest of models to recreate the dynamic behavior of the drill-string is to simplify it as a pendulum. As shown in **Figure 7**, the schematic was created to describe longitudinal and angular vibrations, but not to include lateral vibrations. This schematic also assumes that these types of vibration along the string are independent of each other (Darein and Livesay 1968). The authors of this theory compared their predicted results with rough measurements done to surface equipment and concluded that they were able to "predict reasonably well the overall longitudinal and angular vibration of the drill-string" (Darein and Livesay 1968). However, they recognize the fact that friction is a crucial factor when performing measurements in the field. Another important factor not considered by the authors of this theory is the energy dissipation across the drill-string due to its solid and viscous damping.

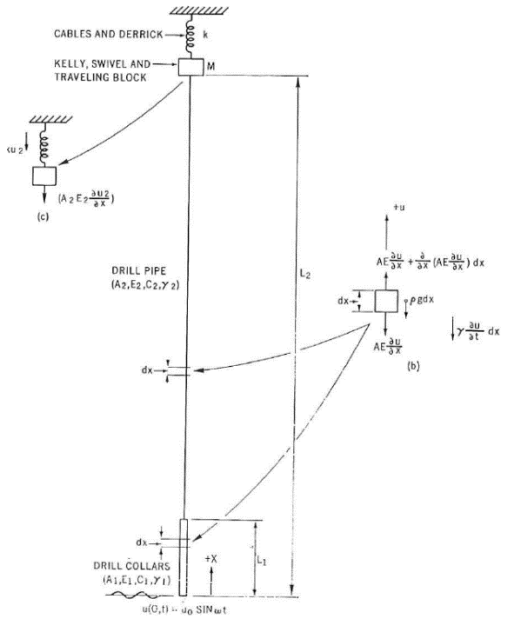

Figure 7. Pendulum type analytical model by Darein and Livesay (1968).

More complex analytical models were developed later, that included more complex system with the purpose of more accurately predicting the dynamic behavior of the drill-string. An example of models like these is shown in **Figure 8**. This type of analytical model is called a "lumped mass torsional model" (Navarro-Lopez and Cortes 2007) (Shor, Pryor and Oort 2014). This type of system describes a torsional model of a drill-string, with each disk representing a drill-pipe. The system increases as the drilling operation advances. Four kinds of elements are described in this model: The top-rotary system, the 'p' number of pipes which are modeled as linear springs of torsional stiffness 'Kt' and torsional damping 'Ct', the bottom-hole assembly which include the drill-collars, and finally the drill-bit (Navarro-Lopez and Cortes 2007). This type of model, although is more precise than the one described earlier, is increasingly complex to solve analytically and simplifications need to be made in order to solve.

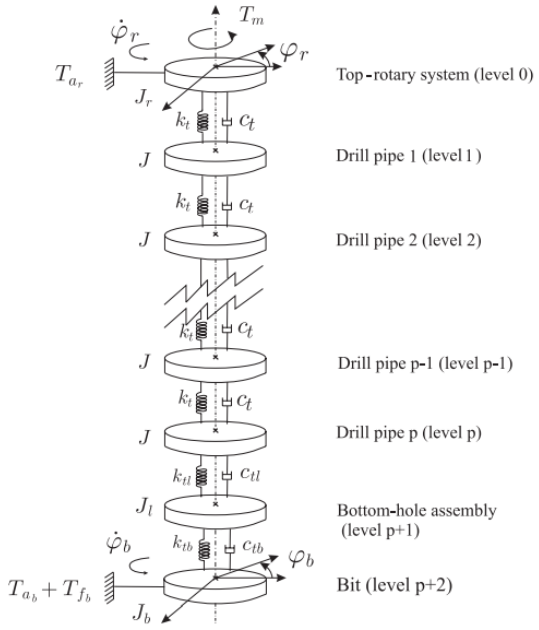

Figure 8. Lumped mass vibration analytical model. (Navarro-Lopez and Cortes 2007)

In horizontal wells, although due to the high friction forces applied to the drill-string vibrations are less severe and energy is more easily dissipated, vibrations are still present and can still cause a significant effect in bottom hole assembly tools. Specially in extended-reach well which are defined by its high horizontal departure ratio to the true vertical depth (Omojuwa, Osisanya and Ahmed 2012). Dynamic analysis has been done to study and understand the behavior of the drill-string in these sections. An example of this type of analysis is shown in **Figure 9**, where the authors take a near straight section of an extended reach well geometry and analyze all the forces involved in section of the string that is in between two stabilizers (Omojuwa, Osisanya and Ahmed 2012). Effects such as torque and drag, buckling and of mechanical vibrations at the BHA are considered in this study.

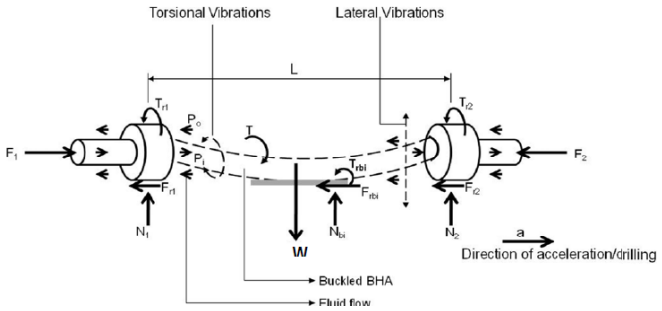

Figure 9. Horizontal String Analytical Model by Omojuwa, Osisanya and Ahmed (2012).

2.2 Finite Element Modelling

The Finite Element Method is a well-known and widely used method to solve mathematical and engineering problems numerically. The use of this method began as early as 1941 in structural engineering with the work by Hrennikoff. Ever since, great advancement in how to use this method to different engineering fields has been developed and the advancement of computational resources and software that we have in the present, has made it more accessible for a wider group of individuals. A wide variety of problems can be solved using this method, including, but not exclusively: structural analysis, heat transfer, fluid flow, mass transport and electromagnetic potential problems (Logan 2012). It is particularly useful when dealing with complicated geometries, material properties and loadings that otherwise analytically are either too complex to solve or they are just outright impossible.

The finite element method is very appealing due to its formulation in a system of algebraic equations instead of requiring to solve systems of differential equations. This method works by fragmenting the system at hand into discrete elements that will be interconnected by vertices called nodal points or simply nodes. Then, instead of solving the physical and mathematical problem for the entire system in one step, the system is

solved algebraically for each node and element to then combine and integrate the overall result (Logan 2012). Although this method saves time by simplifying the problem, there will always be a level of uncertainty associated with this method as the results usually depend on how refined the fragmentation (meshing) of the problem is and how small are the steps increments. Especially, when dealing with a transient analysis, as it is the case for vibration analysis, both the meshing and the selection of the time step is critical to the convergence of the solution.

Finite Element Method applied to non-linear vibrations of the drill-string have been attempted successfully as early as 1978 with the work of Millheim et al. Their study focused on the BHA of the drill-string. In their formulation (shown in **Figure 10**), they simplified the problem by using beam elements and using a uniform grid with simple beam supports and considered four different configurations through the placement of stabilizers shown in **Figure 11** (Millheim, Jordan and Ritter 1978).

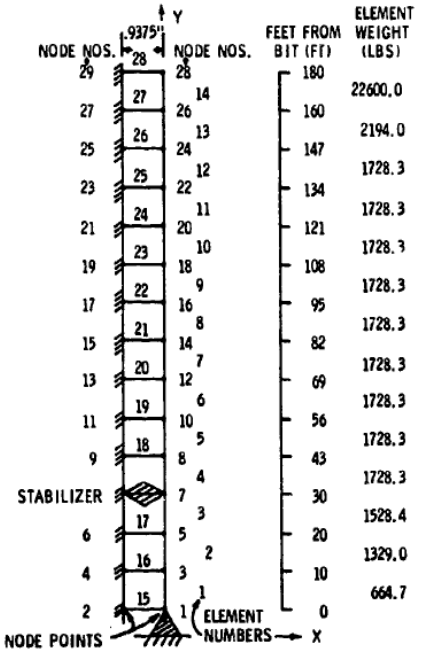

Figure 10. Drill String Simplification for Finite Element Analysis by Millheim, Jordan and Ritter (1978).

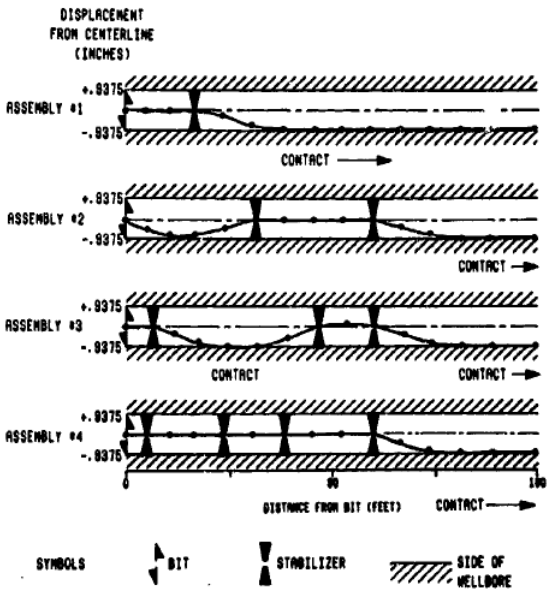

Figure 11. Stabilizer Configurations by Millheim, Jordan and Ritter (1978).

Another important contribution to the study of string dynamics was made by Axisa and Antunes (1992). In their study, they analyze theoretically the effects in linear vibrations of the shaft immersed in a dense annular fluid. The effect of fluid was concluded to have a significant effect in the transverse modes of vibration of the shaft. To solve their analytical model, they created a finite element numerical method. They concluded that stability of the system will have to be studied further in order to accurately predict the dynamic behavior of the string. The analytical system used in their study is shown in **Figure 12** (Axisa and Antunes 1992).

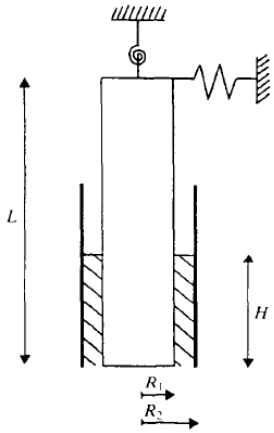

Figure 12. Analytical configuration used by Axisa and Antunes (1992).

Some studies using FEM have focused more on one type of vibration but considering special conditions such as the contact between the wellbore and drill-string. Such is the example of a study made by Spanos et al (2002). They model the BHA considering well borehole contact and their discretization of the model is shown in **Figure 13**. They found good agreement in their results with field data pointing out the uncertainty associated with recording of drill-string vibrations.

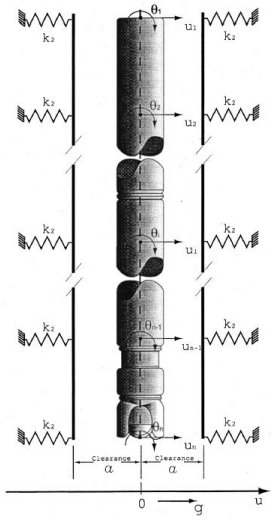

Figure 13. Model Schematics used by Spanos et al (2002).

One of the most recent efforts was made by Kapitaniak et al (2015) where they use a commercial software call ABAQUS for modelling an experimental rig to study the stick-slip phenomena. Their focus was to study the stress and strains associated with the drill-string vibrations in order to compare them with their experimental downscaled model, therefore they modelled their material properties as an anisotropic and flexible material. Their FEM model is shown in **Figure 14** with the respective analytical equivalent. They provided details into their geometry, material and meshing process and conducted experiments to find the equivalent shaft stiffness to use in their model. They compared the results given in the simulation with their experimental setups and the results, they claim were in close agreement. They payed special attention in generating the TOB curves as their focused was on stick-slip vibrations (Kapitaniak, et al. 2015).

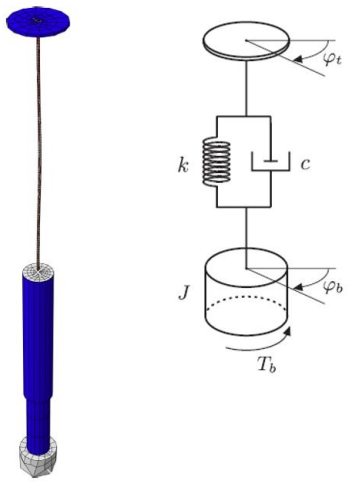

Figure 14. Model Schematic used by Kapitaniak et al (2015).

This procedure followed in this study is worth of recognition as they calibrate their model with experimental downscaled models to accurately predict stick-slip vibration and subsequent mitigation. However, they recognize the fact that in the following steps they need to use a larger setup that it is not as limited to downscaling factors and to the fact

that it can only recreate vertical geometries (Kapitaniak, et al. 2015). Another limitation found in this paper is the fact that they don't study the combined effects of the three modes of vibration. Stick-slip is the most common and usually is a very detrimental type of vibration, but the combined effect of these modes need to be considered in order to accurately predict the behavior of a drill-string and create methods to mitigate them.

Another important research effort was made by Patil (2013). In his study, he developed a mathematical model to study parametrically the stick-slip phenomena influencing factors based on nonlinear differential equations which are formulated considering drill pipes and bottom-hole assembly separately (Patil and Teodoriu 2013). Nonlinear friction forces represented the bit-rock interaction. The analytical model that represents his setup is shown in **Figure 15**. Using the commercial software Simmulink/Matlab they simulated 5,700 m of pipe with a 5 in diameter, and a 180 m BHA with a 6 ¾ in diameter (Patil and Teodoriu 2013).

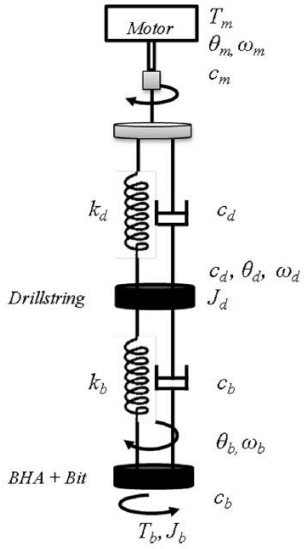

Figure 15. Analytical schematic for model used by Patil and Teodoriu (2013).

From their mathematical model, they concluded that with increasing surface RPMs, stick-slip is converted to torsional oscillations and the ROP is increased. The reduction of WOB decreases the possibility of stick-slip but it naturally decreases ROP at the same time. They also note the importance of considering the drill-string stiffness and inertia when doing a dynamic analysis. They claim that, increasing the stiffness of the drill-string reduces the chance of stick-slip and it increases the ROP. Also, that with increasing inertial mass, it increases the possibility of having stick-slip and reduces the average ROP (Patil and Teodoriu 2013).

2.3 Experimental Research Setups

On the experimental side, there hasn't been as many models as there has been analytical or numerical ones. The obvious reasons are due to the complexity around downscaling several thousand feet of pipe into a lab size space as well as the high cost of the necessary equipment. Most experimental setups won't exceed six-fit tall in height However, there have been several research contributions that have encourage other scientist and engineers to keep pushing the limitation's boundary.

As it was mentioned earlier, one of the latest studies done in this field of study was made by Kapitaniak et al (2015). The numerical method was discussed in the previous section and now the experimental side of it will be discussed.

Their setup was developed at the Centre for Applied Dynamic Research at the University of Aberdeen. As mentioned earlier, their objective was centered in the formulation and validation of a mathematical and numerical model based on experimental formulations. They did not make a downscaled model of a real-case scenario but they achieve making

a testbed for qualitative understanding of detrimental phenomena observed in the industry. The schematic of their experimental setup is shown in **Figure 16**. Their setup aimed to recreate proper conditions of Torque-on-bit (TOB), weight-on-bit (WOB) and more importantly stiffness of the string in order to achieve vibrations such as whirling or stick-slip. To achieve this, they used a flexible shaft consisting of many layers of thin wires. The configuration shown in **Figure 17**, they claim is able to transmit torque while maintaining high flexibility (Kapitaniak, et al. 2015).

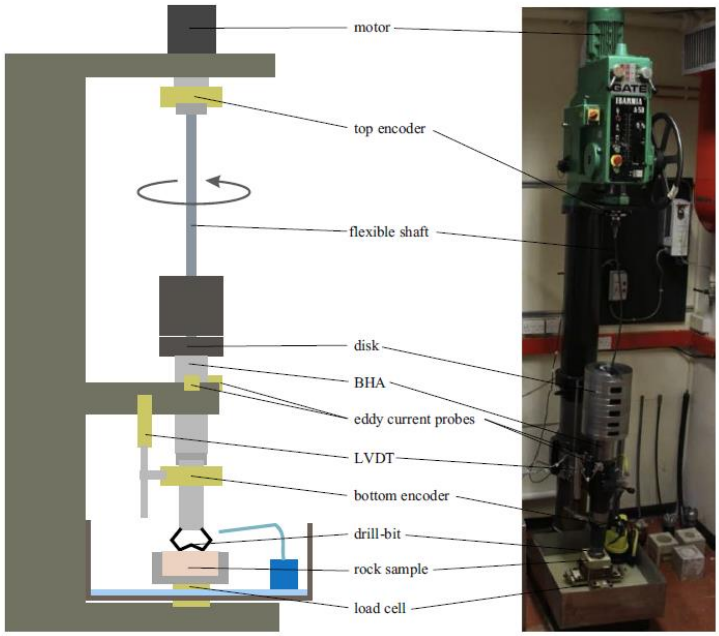

Figure 16. Experimental setup schematic used by Kapitaniak, et al. (2015).

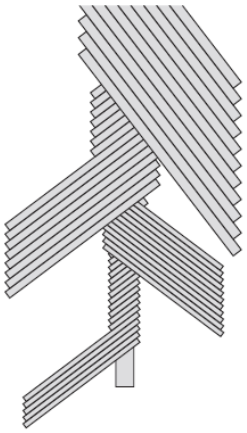

Figure 17. String stiffness schematic used in the setup by Kapitaniak, et al. (2015).

They did used a real bit and rock to study the bit-rock interaction. To do this, they replaced the flexible shaft with a more rigid one and increase the WOB while monitoring the TOB. They found, as expected, that by increasing the WOB, the TOB increased. They also found that the TOB decreases with rotational speed for a short range of speed, to then increase with rotational speed after reaching a threshold (Kapitaniak, et al. 2015).

Westermann et al (2015) presented another very interesting experimental setup. Their setup was to address the gap in scaled model rigs that have been published. They designed a scaled model which has the uniqueness of measuring side-forces during lateral vibrations. They mention that the setup is also designed to test for torsional vibrations as well but no results of this were provided. The setup, shown in **Figure 18**, is one of the longest in length that are available with a combined length of 5.52 m (17.71 ft.). Something they argued, is that it is unpractical to represent the hundreds of meters of pipe of a usual drill-string as, when downscaling, the diameter of the string will be unpractical. Instead, they model critical sections of the BHA and claim to manipulate the torsional stiffness of the drill-string with a torsional spring. They ultimately represent 20 m of a BHA section with an OD of 6.5 in.

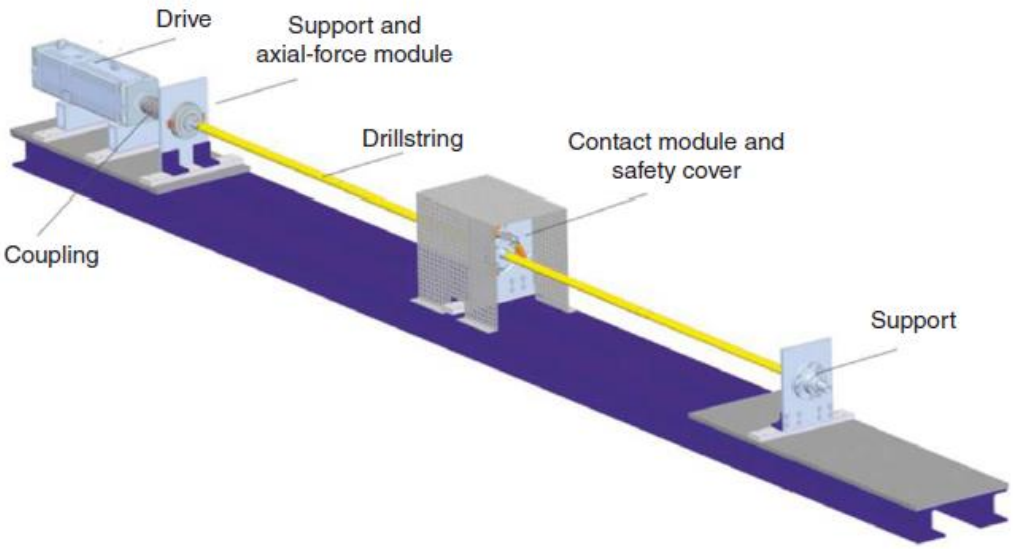

Figure 18. Representation of experimental setup used by Westermann et al (2015).

They were successful in building and testing their experimental setup which measures side forces. They compared their measured data recreating backward-whirl velocity with theoretical rolling velocity and they show that it has good agreement. In a future study not published at the moment this thesis was written they claim that they will show the results of combine effects of whirling and stick-slip.

Another study example of an experimental setup contributing to the understanding of dysfunctional drill-string dynamics was made by Kovalyshen (2014). His main objective was the understanding the root cause of stick-slip vibrations with an experiment using drag bits. The setup is shown in **Figure 19**. Although their results are only preliminary, and no new study has been published by the author relating to this study, he claims that the main factor that causes stick-slip is the bit-rock interaction.

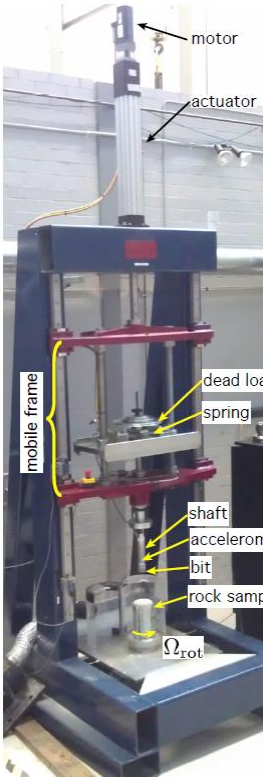

Figure 19. Experimental setup used by Kovalyshen (2014).

Esmaeili et al (2012) contributed with another important experimental work, which focused mainly on the construction and testing of a fully automated laboratory scale drilling rig which they called CDC mini-rig. Their motivation was the lack of vibration recordings in previous research in real-time. They disclosed important information used in their setup (shown in **Figure 20**) such as the length of the drill-string which was 52.4 cm long and 4 cm in diameter. The setup has a maximum WOB capacity of 80 kg on a bit 2 in in diameter, the maximum RPM is 360 and maximum TOB is 30 N.m. They also provide the details of the rock which the drill through while recording the data (Esmaeili, et al. 2012).

Figure 20. Experimental setup used by Esmaeili et al (2012).

They were successful in measuring the drilling parameters while drilling through rock and concluded that WOB and RPM increases ROP as expected. Also, that by keeping WOB constant and reducing rotary speed, both ROP and vibrations decrease (Esmaeili, et al. 2012). The authors of the study made no assertions on the specific modes of vibration and how to mitigate them successfully nor how this will translate to the field.

Another experimental setup, developed by Foster et al. (2010) aimed at quantifying the behavior of an asymmetric vibration damping tool. The setup, shown in **Figure 21** use a DC motor and a steel rod of 5 mm in diameter. The length of the drive ranges from 250 mm to 2000 mm. The maximum WOB used was 4.5 Kg and an inertia wheel was used to simulate the BHA. To simulate torsional vibration the inertial wheel was used to represent the top drive in addition to the one representing the BHA and a 1 mm diameter high

tensile steel wire was used to represent the drill-string. A drill bit of 8 mm diameter was located at the BHA contacting a steel bore (Foster, Macfarlane and Dinnie 2010).

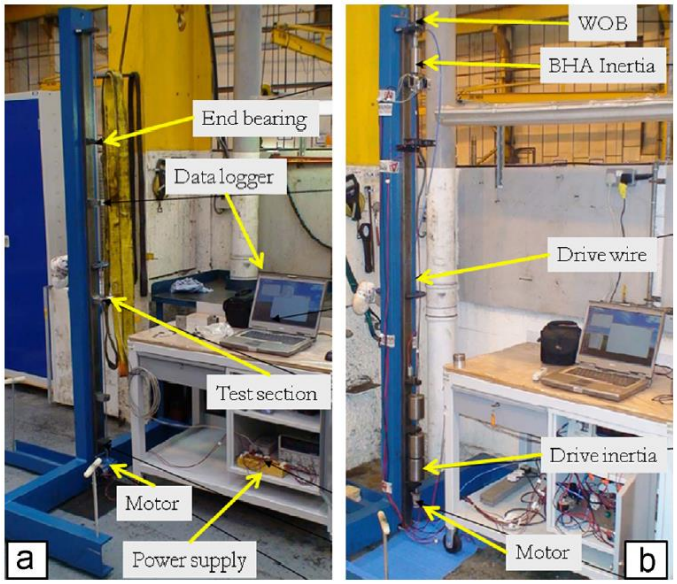

Figure 21. Experimental setup used by Foster et al. (2010).

The authors of this study were testing the Asymmetric Vibration Tool (AVDT) which they concluded an analysis of advantages and disadvantages on using this tool in the field. They claim that their field test showed improvement in torsional vibrations by using a AVDT but that attention must be paid to the BHA (Foster, Macfarlane and Dinnie 2010). As discussed earlier, Patil (2013) developed a mathematical model, presented in Patil and Teodoriu (2013) where he studied parametrically the effects of drilling parameters on stick-slip. After completing this effort, they proceeded to build a downscaled model which they designed using the 'law of similitude' which we'll refer to it later. They considered the BHA, which consists of downhole measurement tools, undergoes more sever vibration than the drill-string above. This setup is shown in **Figure 22**. They downscaled 150 m of length of a BHA to a 5 m laboratory setting for testing. The string used was 6 mm OD and 4 mm ID. Instead of using a rock and bit as other researchers,

they used a breaking device to recreate the non-linear interaction at the bit. Patil (2013) shows the results of using different materials to recreate the best stiffness possible in which is showed in the field. For his setup, he concluded that for stick-slip the material PVC was the best in terms of torsional stiffness.

Figure 22. Experimental setup used by Patil (2013).

A comparative review of the experimental setups since 2003 until present was taken from Patil (2013), corrected and expanded to include the latest developments in experimental setups is presented in the Appendix A. This table includes the main focus of the investigation, the approach, the setup details and their limitations.

2.4 Current Experimental Setups Limitations

Although all of the presented experimental setups have contributed to the understanding of dysfunctional drill-string and BHA dynamics, there are still some setbacks that are going to be addressed in the proposed setup of this thesis.

The first limitation it is the dimensional limitations. As Westermann et al (2015) explains in their work, oftentimes experimental setups do not attempt to do a mechanical downscaling of field conditions. This is due to the fact that downscaling directly thousands of feet of drill-pipe to very limited and expensive lab space, it's just impossible for most researchers. The largest downscaled setup build to date is 5.4 m (17.7 ft.) in length. This makes it nearly impossible to later upscale results and predict more accurately what could be seen in the field and come up with more consistent preemptive methods. This limitation is to be addressed with the new proposed setup later presented in this work.

The second limitation observed in the experimental setups studied by the author is that they have only addressed vertical wells. With increasing numbers of directional, horizontal and extended reach wells for the successful production of unconventional reservoirs, there is a gap in the research done up to date to study the dynamics of the drill-string with different well geometries. The proposed setup in this work will be designed to not only study vertical configuration wells, but also vertical and horizontal, and eventually 'S' type wells. The advantage that is presented at the University of Oklahoma is the laboratory space available for this study. The new proposed setup will account with a unique flexibility in the well configuration that can be represented.

The third limitation of the available experimental setups is the ability to accurately reproduce bit-rock interactions. There has been some debate in the topic on whether or not to use real rocks with downscaled drill bits in the setups to study and predict vibrations. The author of this work believes that the current studies that use drill bits do not reflect the vibration modes of real size bits, and therefore this may lead to inaccurate reproduction of rock-bit interactions. To overcome this problem, the new proposed setup will use a high frequency hexapod and an electromagnetic break which will allow to recreate a wide spectrum of bit-rock interaction behavior. The reason why a hexapod could prove more advantageous versus a normal vibratory table, is the fact that in order to recreate the bit-rock interaction, an extremely high precision of repeating movements is needed. The hexapod used in the proposed setup have a strut resolution of 50 nano meters, with up to 4g acceleration and 250 mm/s speed. It is expected that this hexapod will be able to recreate most severe bit-rock interaction processes.

Chapter 3: Finite Element Modeling

Finite Element Method as described in Chapter 1 it is an incredibly useful tool for engineers and researchers across any field. It provides the means to analyze complex non-linear problems and obtain results in a short period of time providing a sense of the expected outcome in reality. As such, it was decided to use this tool through a widely used and powerful engineering software called Ansys Workbench V17.1. Two sets of finite element analysis are presented in this work.

The first it's a published study in the SPE Health, Security, Safety, Environment and Social Responsibility Conference North America 2017 which was held on 18th to the 20th of April in New Orleans, Louisiana (SPE-184420-MS). In this first study a real size BHA is used and the three modes of vibration (torsional, lateral and axial) are applied to the string in six different configurations. The BHA response according to its deformation are compared.

The second study is related to what was observed from the first study but it is applied to the vertical configuration of the experimental setup presented in a later section.

3.1 Bottom-Hole-Assembly FEA Study

This study was published by myself, Emmanuel Omojuwa PhD candidate at the University of Oklahoma and Dr. Catalin Teodoriu Associate Professor at the Mewbourne School of Petroleum and Geological Engineering of the University of Oklahoma. The objective of this study was to perform a Finite Element Analysis on a real size BHA to observe the response by applying the three modes of vibration described in Chapter 1.

3.1.1 Simulation Setup

As mentioned before, the commercial software Ansys Workbench V 17.1 was used to perform this analysis. A transient analysis was selected as a base for the analysis as the response over a finite period of time was required.

A BHA geometry was designed in the commercial software for CAD modelling called Solidworks 2016 and can be seen in **Figure 24**. For this study, three stands of two drill collars were used, as well as two stabilizers located in between each stand. The summary of the dimensions used can be seen in **Table 1** (Marquez, Omojuwa and Teodoriu 2017).

Table 1. Dimensional setup used in model by Marquez, Omojuwa and Teodoriu (2017).

Component	Length	OD	ID
Drill Collar	30 ft.	6.25 in	2.81 in
Stabilizers	3 ft.	8.5	6.25
Bit	1 ft.	8.5	-

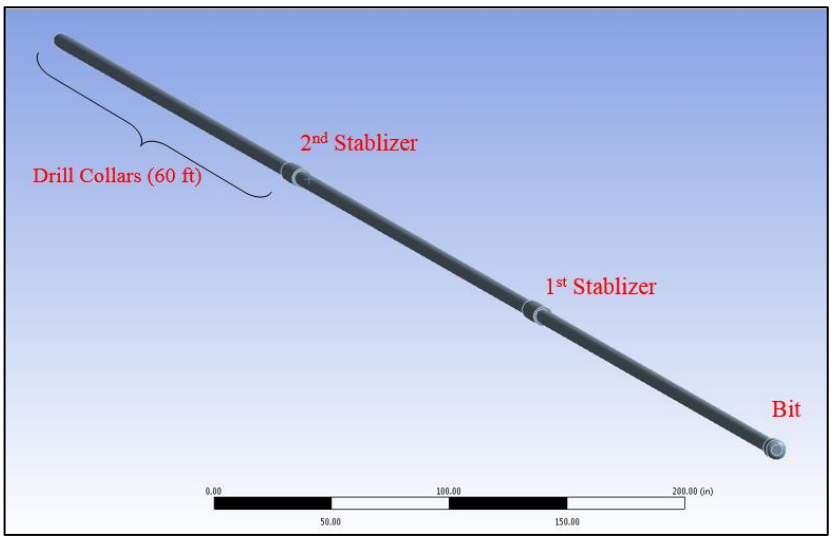

Figure 23. Model setup used by Marquez, Omojuwa and Teodoriu (2017).

A critical consideration made for this study was to not include the wellbore geometry. The first reason is for the authors wanted to see the unaltered behavior of the string when the three modes of vibrations are coupled into a single analysis. This allowed for any movements of the string not to be altered or mitigated due to this condition. The second reason was oriented towards computational resources available for this study. Including an external body to the analysis that does not have any initial contact with the system will transform the analysis to a collision plus a non-linear dynamic analysis. This requires a tremendous amount of computational resources and the lack of previous studies to compare results to made it unbeneficial to even try to attempt this.

Of course, the authors and myself are aware that the wellbore friction has a critical effect on vibrations and that it's something that in follow up studies should be considered. However, the results of this finite element analysis are not quantitative but qualitative.

3.1.2 Meshing and Boundary Conditions

For the meshing in this analysis a curvature type size function was used with tetrahedron shape elements. The final count of elements was 36,115 with 70,724 nodes. Considering the size and proportions of the geometry the resolution and refinement of this mesh was considered to be sufficient (Marquez, Omojuwa and Teodoriu 2017). Additionally, the material for the string was structural steel available through the material's library preloaded into Ansys's Engineering Library.

Careful attention was paid to the boundary conditions applied to this model. As no other finite element model has coupled the three modes of vibration in a single analysis, there was little to no way of comparing initial conditions for the system. As such, six cases were presented. The summary of the studied cases is shown in **Table 2** with the respective

magnitudes for the torque, axial load and displacements shown in **Table 3**. To recreate torsional vibrations, a torque of 40,000 lbf was used and applied in a sinusoidal function at an angular velocity of 120 rpm for the base case 1. An axial load of 20,000 lbf to recreate the WOB was applied as well as a sinusoidal function to recreate the bit bouncing. Finally, the lateral disturbances were applied as displacements with a constant value of 1.2 in and applied as well with a sinusoidal function. Different attempts were made to find the best configuration of lateral displacements (Marquez, Omojuwa and Teodoriu 2017). At the end, the best configuration resulted in having a phase difference of 90 degrees between the time of application. The lateral vibration response observed was more realistic when this configuration was applied with the singular exception of uniplanar whirling which happens if no torsional vibration is present.

Later, the rest of the cases presented were variations of different load configurations to study how the magnitudes of this loads affected the overall vibration response.

Table 2. Summary of cases modeled and presented by Marquez, Omojuwa and Teodoriu (2017).

Case	Torque function	WOB function	Lateral disturbance in X axis	Lateral disturbance in Z axis
1	*Torque x Sin (wt)*	*Axial Load x Sin (wt)*	*Displacement x Sin (wt)*	*Displacement x Sin (wt+90°)*
2	*Torque/2 x Sin (wt)*	*Axial Load x Sin (wt)*	*Displacement x Sin (wt)*	*Displacement x Sin (wt+90°)*
3	*Constant Torque*	*Constant Load*	*Displacement x Sin (wt)*	*Displacement x Sin (wt+90°)*
4	*Torque x Sin (Kwt)*	*Axial Load x Sin (wt)*	*Displacement x Sin (wt)*	*Displacement x Sin (wt+90°)*

5	*Torque/4 x Sin (Kwt)*	*Axial Load x Sin (wt)*	*Displacement x Sin (wt)*	*Displacement x Sin (wt+90°)*
6	*Torque x Sin (Kwt)*	*Axial Load/2 x Sin (wt)*	*Displacement x Sin (wt)*	*Displacement x Sin (wt+90°)*

Table 3. Magnitude values used in simulation used by Marquez, Omojuwa and Teodoriu (2017).

Torque	3,333.3 ft.lbf (40,000 lbf in)
Load	20,000 lbf
Displacement	1.2 in
Angular velocity (w)	120 rpm
Time (t)	Variable
K	Random value between 0 and 1

For the time step selection of the analysis, a time step of 0.02 seconds was required in order to cover the full spectrum of the load application without any observing any peak truncation. Due to this restriction, a total analysis time of 6 seconds was performed to balance the computational resources and time taken to perform the full analysis. However, it was determined that this time was sufficient to observe the desired response (Marquez, Omojuwa and Teodoriu 2017).

Finally, a fixed support restriction was placed at the top of the BHA in order to conduct the transient analysis properly. Frictionless supports were placed around the stabilizers which assumes ideal contact between the wellbore and stabilizers which is not of course, what is observed in the field.

3.1.3 Results and Analysis

The first set of results presented were the comparison of maximum total deflection of the geometry as it is shown in **Figure24**. As it can be seen, for Case 3 which had constant loads and oscillating displacements, the amplitude of the vibrations was significantly

larger than for any other simulated case. Case 1 (base case) presented a smaller amplitude of the vibration and a shorter frequency than for Case 3. For Case 4, which applied a random alternating torque, the behavior was not significantly different than for Case 1 but a small shift to the right of the vibration response. Case 2, which halved the torque applied in the base case, presented a higher initial peak but the frequency of the vibration responses increased. Finally, for Case 5 and Case 6, no considerable difference was observed when compared to Case 2 (Marquez, Omojuwa and Teodoriu 2017).

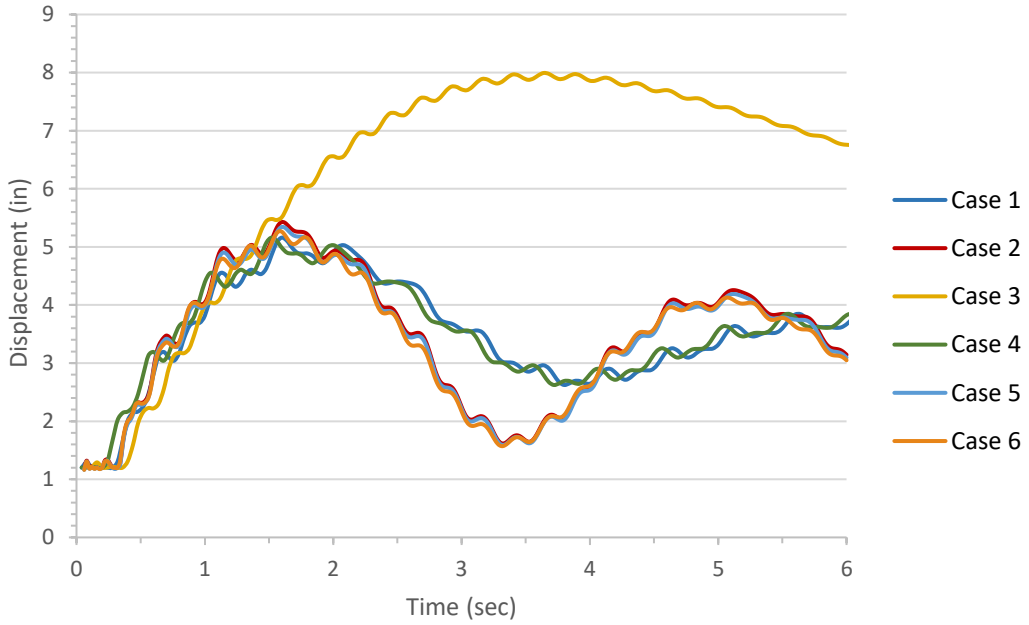

Figure 24. Maximum total deformation. (Marquez, Omojuwa and Teodoriu 2017)

Next set of results presented were the maximum lateral deformations located between the bit and the first stabilizer. No significant deformations were observed in the second, nor the third stand of drill collars. This is due to the boundary condition of ideal frictionless wellbore geometry which is not what it is seen in the field. These results which represent a type of lateral vibration response can be seen in **Figure 25**.

As it can be seen, for Case 3, the amplitude of the vibrations was the largest of the six cases and the frequency of the maximum amplitude decrease, similar to what was seen in the previous set of results. For cases 1 and 2, a very similar frequency is observed but the magnitude of magnitude differs. The magnitude of the lateral displacements of this section increases as the torque applied decreases. A possible explanation for this phenomenon is the energy distribution in the string during different load application. When only one mode of vibration is induced, the magnitude of the vibration response is larger and the frequency gets smaller in comparison when more modes are coupled in conjunction. This is clear when comparing Case 1,2 and 3. For Case 6, very similar results were observed in comparison with Case 2 and 4 which is why Case 4 was not included in this figure (Marquez, Omojuwa and Teodoriu 2017).

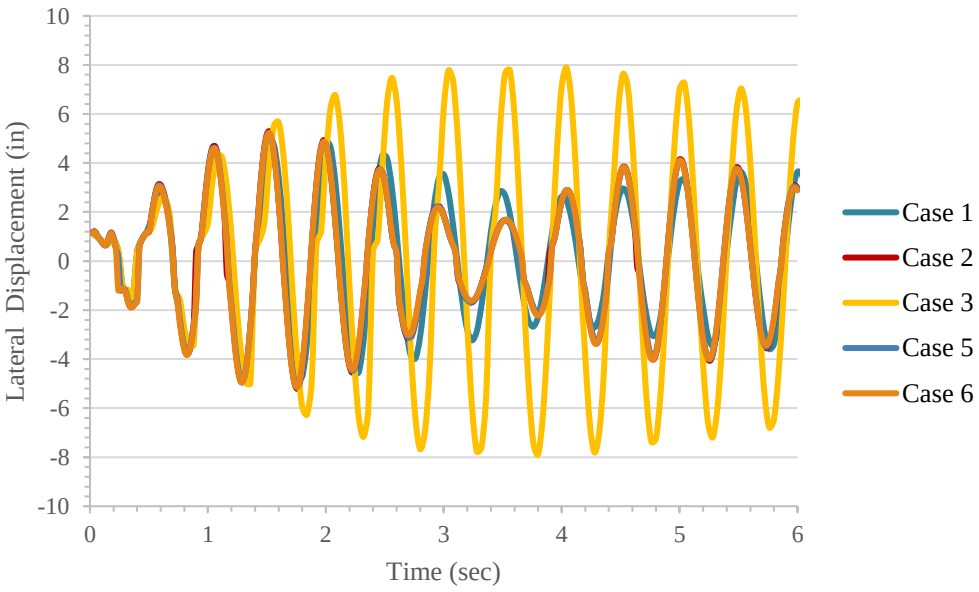

Figure 25. Maximum lateral deflection of first stack. (Marquez, Omojuwa and Teodoriu 2017)

Finally, the axial vibration response is studied and represented in **Figure 26**. A similar behavior in comparison with the previous set of results was observed. When one mode of vibration was induced, the magnitude of the vibration response was considerably higher than when all three modes were induced. For cases 1 and 2, another similar behavior was observed with the amplitude of the axial displacement varying but not considerably. Finally, for case 6 it can be seen that the axial vibrations will mitigate, as expected when reducing the WOB. Case 4 yielded identical results as 2 once again so it was not included in the figure (Marquez, Omojuwa and Teodoriu 2017).

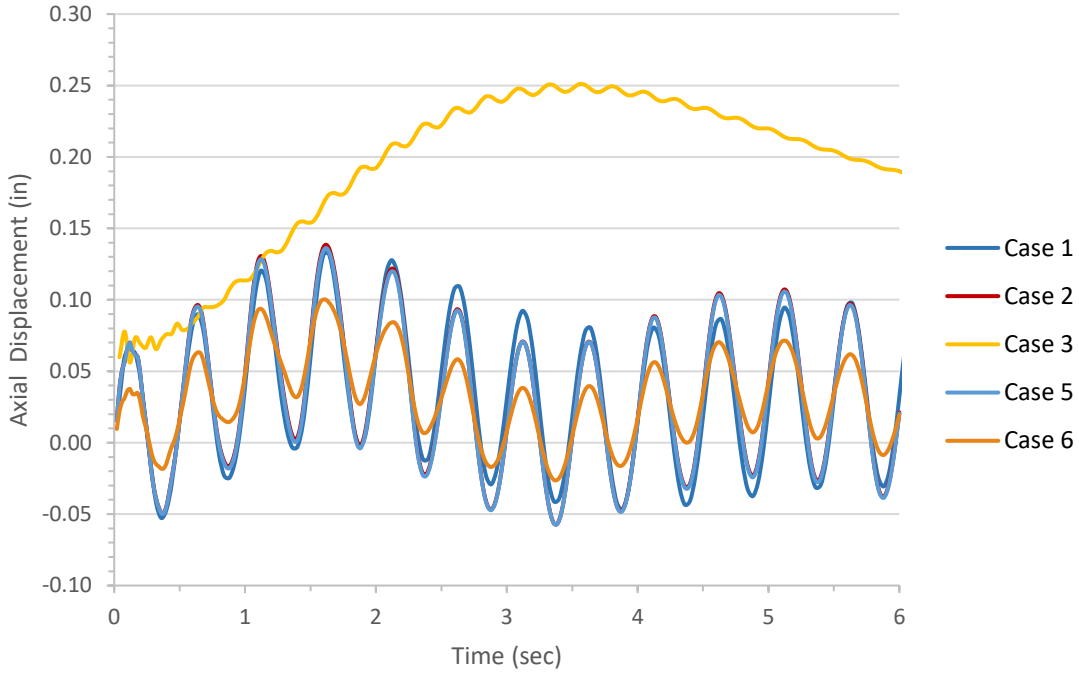

Figure 26. Axial deflection of bit. (Marquez, Omojuwa and Teodoriu 2017)

3.1.4 Conclusions

It was concluded that first, the Finite Element Analysis does allow the representation and modeling of dynamic response of the drill-string. The location of critical areas where vibrations will propagate and the magnitude of these vibration can be observed from these

analyses. The qualitative analysis of this study showed that if only one type of vibration is being considered, the magnitude of the other modes of vibration will increase significantly. For more comparable results, the three modes should be studied at the same type unless a particular desired for studying a mode of vibration is pursued. The combination of these modes of vibration seems to lead to a reduction of overall magnitude of vibration responses, which could point toward the application of new downhole vibratory tools to mitigate these dynamic dysfunctionalities (Marquez, Omojuwa and Teodoriu 2017).

3.2 Experimental Setup FEA Study

The second Finite Element (FEA) study was created after the published study presented in the previous section. As the experimental setup presented in a later section will have downscaled parameters for all of its components, a finite element analysis was required to corroborate the consistency of the previous study and conclusions. As such, a similar study using the finite element method was made with similar conditions, yet expanded, for the drill-string that will be part of the experimental setup.

For this study, once more Ansys Workbench V 17.1 was the commercial software used to perform a transient structural analysis. Four different materials are used: aluminum, structural steel polyethylene (PE) and polyvinyl chloride (PVC). Two different sets of loadings were used for each material. The first set is with only inducing lateral vibrations, keeping the torque and WOB on the string constant, while the second set all modes of vibrations were included. Additionally, a modal analysis of these four materials is

presented comparing the first 140 modes of vibration for this geometric configuration, identifying which frequencies will create resonance with each mode of vibration.

3.2.1 Simulation Setup

The geometry for this study was created again using the commercial software Solidworks 2016 and can be seen in **Figure 27**. This is the simplified version of the geometry of the drill-string that will be used in the experimental setup presented in a future section. The dimensions of the setup are summarized in **Table 4**.

Table 4. Dimensional considerations for experimental setup modelling.

Component	Length	OD
Drill String	41 ft.	0.125 in
Top Holder	0.394 in	0.250 in
Stabilizer	0.394 in	0.250 in
Bit	0.394 in	0.250 in

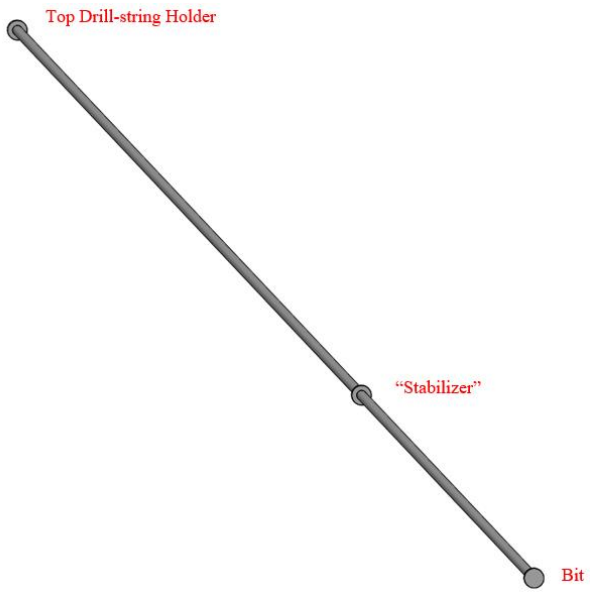

Figure 27. Geometry configuration used for experimental setup modelling.

Similar considerations were made as in the previous presented study (Marquez, Omojuwa and Teodoriu 2017), including to not consider the wellbore geometry in the analysis. To reiterate the argument that it is desired to observe the unaltered behavior of the string without including collision analysis between the string and the formation.

3.2.2 Material Properties

As mentioned, four materials were originally tested. These materials are: structural steel, aluminum, polyethylene (PE) and polyvinyl chloride (PVC). The properties of the first three materials were obtained from the software Ansys V17.1 material's library. The structural steel and aluminum material properties were retrieved from the non-linear library and the polyethylene material properties were retrieved from the general materials library. The PVC material properties were obtained from different websites were the values for its most important properties did not change. The material properties for the metals can be seen in **Table 5** and for the plastics on **Table 6**. It was observed that the properties of the non-linear materials (steel and aluminum) had no relevant properties for the analysis. Therefore, only the relevant material properties are presented.

Table 5. Material properties for metals used for this model.

	Structural Steel				**Aluminum**			
	SI units		Standard units		SI units		Standard units	
Density	*7850*	*Kg/m3*	*490.06*	*lb/ft3*	*2770*	*Kg/m3*	*172.93*	*lb/ft3*
Young's Modulus	*2.00E+11*	*Pa*	*2.90E+07*	*psi*	*7.10E+10*	*Pa*	*1.03E+07*	*psi*
Poisson's Ratio	*0.3*	*-*	*0.3*	*-*	*0.33*	*-*	*0.33*	*-*
Bulk Modulus	*1.67E+11*	*Pa*	*2.42E+07*	*psi*	*6.96E+10*	*Pa*	*1.01E+07*	*psi*
Shear Modulus	*7.69E+11*	*Pa*	*1.12E+08*	*psi*	*2.67E+10*	*Pa*	*3.87E+06*	*psi*

Table 6. Material properties for plastics used for this model.

	Polyethylene				Polyvinyl Chloride			
	SI units		Standard units		SI units		Standard units	
Density	*950*	*Kg/m3*	*59.307*	*lb/ft3*	*1400*	*Kg/m3*	*87.399*	*lb/ft3*
Young's Modulus	*1.10E+09*	*Pa*	*1.60E+05*	*psi*	*2.00E+09*	*Pa*	*2.90E+05*	*psi*
Poisson's Ratio	*0.42*	*-*	*0.42*	*-*	*0.4*	*-*	*0.4*	*-*
Bulk Modulus	*2.29E+09*	*Pa*	*3.32E+05*	*psi*	*3.33E+09*	*Pa*	*4.83E+05*	*psi*
Shear Modulus	*3.87E+08*	*Pa*	*5.62E+04*	*psi*	*7.14E+08*	*Pa*	*1.04E+05*	*psi*

3.2.3 Meshing

The meshing for this study was made considerably different than for that of the previous study. Being the geometry considerably slenderer, meaning that the length/OD ratio was too large, the same approach for the meshing could not be made. Tetrahedron elements deformed the geometry considerably and the quality of the mesh and aspect ratio was not acceptable. As such, a sweeping type of meshing was used. This allowed for a more uniform meshing around small cylindrical elements throughout the drill-string, increasing the quality considerably of the mashing and having an aspect ratio of acceptable ranges. An example of the meshing used can be seen in **Figure 28**. Given that the time step for this analysis was considerably small (0.01 sec) and that the analysis was run for 9 seconds, yielding 900 loading steps, the mesh was designed to have the least number of elements and nodes as possible. The final statistical values for the mesh were 64,736 nodes and 12,226 elements.

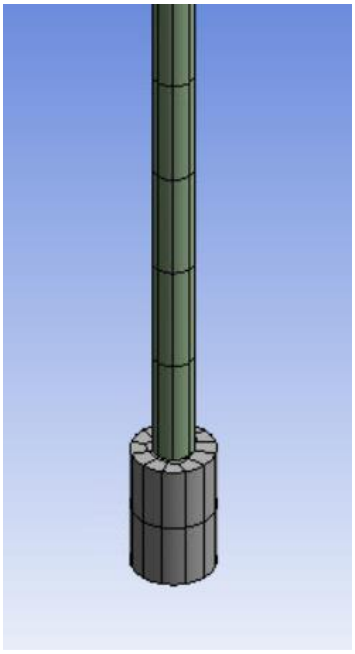

Figure 28. Sweeping mesh along the drill-string.

3.2.4 Boundary Conditions

In order to accurately compare the behavior of the three selected materials and two different sets of boundary conditions, the loading conditions remained constant for all of the simulated cases. The two different configurations, are related to what was observed in the previous presented study where, the higher vibration responses were observed when only one type of vibration is induced in the system. The magnitudes and sets of boundary conditions are summarized on **Table 7**. These loads were applied at the bit. The frequency chosen for this analysis was 250 rpm (26.18 rad/s) and a maximum analysis time of 9 seconds and a time step of 0.01 s.

Table 7. Magnitudes for Boundary Conditions

	1st Set: "Only Displacements"	**2nd Set:** "All modes"
Torque (lbf ft)	*0.01*	*0.01 x Sin (wt)*
Weight-on-bit (lbf)	*0.01*	*0.01 x Sin (wt)*
Lateral Displacements (in)	*0.02 x Sin (wt)*	*0.02 x Sin (wt)*

The movement conditions set in this analysis are similar to the previous study. A fixed support type restriction was placed at the 'top drill-string holder' and a frictionless type support was placed at the 'stabilizer'.

3.2.5 Special Analysis Considerations

Besides the important considerations of not including a borehole to not restrict the unaltered behavior of the drill-string and avoid modeling with a highly complex collision analysis, other important considerations were made for this analysis. Firstly, fluid will not be included in this particular analysis. Even though in the field, the drill string will be surrounded by drilling fluid, for the purpose of this analysis it was desired to investigate the unaltered behavior of the drill-string when coupled modes of vibration are applied. It is expected that, if fluid is included in the system, the viscosity of the fluid will have a significant effect on the damping of the vibrations, mitigating the overall response.

Secondly, in the analysis settings of the transient analysis, the option of 'large deformations' was activated. The help and guide section of Ansys V 17.1 recommends to activate this option if the body is slender and offers a rule of thumb which states: "… you can use large deflection if the transverse displacements in a slender structure are more than 10% of the thickness". When this option is activated, the software will take into account stiffness changes resulting from change in element shape and orientation due to large deflections.

Thirdly, in the analysis settings in the damping controls, a value for the numerical damping of 0.1 was used as well as a value of 0 for both the stiffness and mass coefficients. After reviewing extensively, the damping "Rayleigh model" (Review

section 1.3.2) that Ansys V 17.1 uses for non-linear analysis, it was decided that a common initial value for the numerical damping of 0.1 was a good first assumption given that experimental data is lacking. Once the experiment for this setup is made, a "Damping vs. Frequency" data can be obtained and used as input for the software's analysis. The argument for using 0 for both stiffness and mass coefficients is related to what was explained in section 1.3.2. These values have a very significant impact on non-linear models and particularly on models where the stiffness changes. Even after several trials and errors in this study, it was found that the analysis did not converge with any of the attempted given values. Therefore, it is highly recommended to input these after experimental data is available and not to use the trial and error approach.

Finally, in the solver settings of this analysis, a 'Direct' type of solver was selected. The argument for using this type of solver is that, given the time step of 0.01 sec the analysis was already taking almost 8 hours on average to complete. Usually, using the alternative 'Iterative' option will increase the solving time significantly and it is only recommended when using a relatively large time step. Also, with a considerable small time step, it is expected that the effects of an iterative solver will not turn as beneficial.

3.2.6 Modal Analysis

The first step in this study is to find and compare the different modes of vibration for each material and identifying which modes will create resonance with which modes of vibration. Ansys V17.1 modal analysis was used to perform this analysis. The first 140 modes of vibration where simulated and retrieved for comparison. The criteria for using 140 modes was to find at least 1 natural frequency for torsion and 1 for axial vibration.

In general, most natural frequencies found were for lateral vibrations with different frequencies of sinusoidal oscillations.

On **Table 8** are summarized the principal natural frequency for each mode as well as the frequencies and modes of vibration at which each mode will resonate. As it can be seen, for lateral, torsion and axial, all the materials have similar modes at which the system will come into resonance. However, the frequencies at which this occurs are different when comparing aluminum and steel with PE and PVC. There is a large discrepancy of frequency where the systems with aluminum and steel will enter resonance for torsion and axial vibrations compared with the PE and PVC frequency. This may lead to a large discrepancy in the results for the simulation of these materials by applying the same boundary conditions.

Table 8. Summary of Modal Analysis

		Lateral at bit		Torsion		Axial	
Material	**Fundamental (Hz)**	**Mode**	**Frequency (Hz)**	**Mode**	**Frequency (Hz)**	**Mode**	**Frequency (Hz)**
		1	*0.1269*	*77*	*60.789*		
Aluminum	*0.1269*	*2*	*0.1275*	*137*	*184.05*	*100*	*100.78*
		1	*0.1266*	*77*	*61.301*		
Steel	*0.1266*	*2*	*0.1268*	*137*	*185.6*	*100*	*100.48*
Polyethylene (PE)	*0.0269*	*1*	*0.0269*	*75*	*12.504*	*100*	*21.421*
		2	*0.0271*	*133*	*37.859*	*116*	*28.698*
Polyvinyl Chloride (PVC)	*0.0301*	*1*	*0.0301*	*77*	*13.988*		
		2	*0.0302*	*133*	*42.351*	*100*	*23.794*

The modes of natural frequencies can be seen in **Figure 29**. As it can be seen, from the first 140 modes of natural frequencies, the steel and aluminum are almost overlapping throughout the range of frequencies. It can also be seen the large discrepancy discussed between the range of frequencies of the steel and aluminum and the PE and PVC.

However, even though the steel and aluminum are overlapping, the PE and PVC are only close to each other and toward the end, it can be seen how they start to diverge from each other with the PVC having higher natural frequencies for the same mode of vibration.

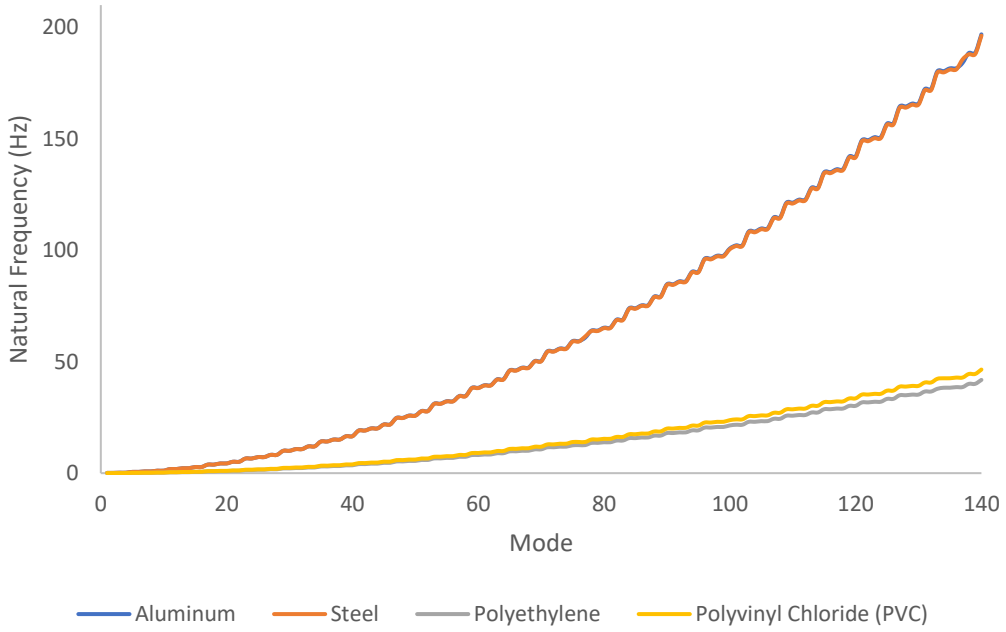

Figure 29. Results of the first 140 modes of natural frequencies.

Again, this discrepancy in range of frequencies might result in a large discrepancy of results of the simulated models between the metals and plastics.

3.2.7 Results and Analysis

After performing the simulation for the four materials and two configurations the first that was noticed was the impossibility to compare the metallic materials with the plastic ones. As predicted from the modal analysis, by applying the same boundary conditions to both polyethylene (PE) and Polyvinyl Chloride (PVC), it was noticed that the deformation diverges as the pipe buckles and collapses due to extremely high deformations. The set of results for the metallic materials was considerable better and

went in accordance to what was expected with the established conditions. 12 different configurations of loadings were attempted to the PE and PVC in order to obtain comparable results. The criteria for obtaining good comparable results was to observe vibrations with at least one period of oscillation in order to be able to quantify the results. A summary of the attempted configurations for the plastic materials is shown in **Table 9**. It is worth noting that the WOB and Torque were applied constant and the displacements were applied in a sinusoidal function. The reason for this is because it is expected that the configuration with only one mode of vibration and the other two modes constant, the deflections will be considerably higher than for the case with all modes of vibration. Given this, if this configuration did not show observable vibrations or it buckled beyond considerable limits, then there will be no point in performing the configuration with all modes of vibration nor redoing the metal materials simulations with new magnitudes for the loading.

Table 9. Attempted configurations for the PE and PVC.

Attempt	Configuration	Boundary Conditions		Observation
1	**Polyethylene (PE)**	*WOB (lbf ft)* *Torque (lbf)* *Displacements (in)*	*0.01* *0.01* *0.02*	The deformation diverges with excessive deformation. Structure buckles and collapses.
2	**Polyethylene (PE)**	*WOB (lbf ft)* *Torque (lbf)* *Displacements (in)*	*0.005* *0.01* *0.02*	The deformation diverges with excessive deformation. Structure buckles and collapses.
3	**Polyethylene (PE)**	*WOB (lbf ft)* *Torque (lbf)* *Displacements (in)*	*0.001* *0.008* *0.008*	The drill-string shows high initial deflection but immediate stabilization showing no vibrations.
4	**Polyethylene (PE)**	*WOB (lbf ft)* *Torque (lbf)* *Displacements (in)*	*0.005* *0.008* *0.008*	The drill-string shows high initial deflection and then a decrease in deflection but no second vibration peak was observed
5	**Polyvinyl Chloride (PVC)**	*WOB (lbf ft)* *Torque (lbf)*	*0.01* *0.01*	The deformation diverges with excessive

		Displacements (in)	*0.02*	deformation. Structure buckles and collapses.
6	**Polyvinyl Chloride (PVC)**	*WOB (lbf ft)* *Torque (lbf)* *Displacements (in)*	*0.005* *0.01* *0.02*	A deformation peak is observed but no considerable subsequent peak was observed.
7	**Polyvinyl Chloride (PVC)**	*WOB (lbf ft)* *Torque (lbf)* *Displacements (in)*	*0.005* *0.008* *0.008*	A deformation peak is observed but no considerable subsequent peak was observed. Magnitudes are just lower than previous configuration.
8	**Polyvinyl Chloride (PVC)**	*WOB (lbf ft)* *Torque (lbf)* *Displacements (in)*	*0.0075* *0.008* *0.008*	The deformation diverges with excessive deformation. Structure buckles and collapses.
9	**Polyvinyl Chloride (PVC) with steel bit**	*WOB (lbf ft)* *Torque (lbf)* *Displacements (in)*	*0.01* *0.01* *0.02*	The deformation diverges with excessive deformation. Structure buckles and collapses.
10	**Polyvinyl Chloride (PVC) with steel bit**	*WOB (lbf ft)* *Torque (lbf)* *Displacements (in)*	*0.005* *0.01* *0.02*	A deformation peak is observed but no considerable subsequent peak was observed.
11	**Polyvinyl Chloride (PVC) with steel bit**	*WOB (lbf ft)* *Torque (lbf)* *Displacements (in)*	*0.005* *0.008* *0.008*	A deformation peak is observed but no considerable subsequent peak was observed.
12	**Polyvinyl Chloride (PVC) with steel bit**	*WOB (lbf ft)* *Torque (lbf)* *Displacements (in)*	*0.005* *0.0075* *0.004*	A deformation peak is observed but no considerable subsequent peak was observed. Magnitudes are just lower than previous configuration.

Therefore, it was decided to excluded from the result comparisons. However, it was desired to investigate the cause of this significant discrepancy in behavior from what was observed with the steel and aluminum. The first instinct of the root of this behavior is the stiffness and mass of each of these material configurations. It was decided to calculate theoretical axial, radial and torsional stiffness for a section of a pipe with the same geometrical parameters and only changing the material.

To calculate the axial stiffness for each material, the following expression was used,

$$K_{axial} = \frac{EA}{L}$$

Where, E is the Young's modulus, A is the cross-sectional area and L is the length of the rod.

Then, to find the radial stiffness two possibilities were considered. In beam theory, for a cantilever beam which is fixed on one end but not the other, there are two possible stiffness values. If the free end is allowed rotation then the expression results in,

$$K_{radial} = \frac{3EI}{L^3}$$

Where I, is the inertia of the cross-sectional area. If that end is only allowed displacement but not rotation, then the following expression is used,

$$K_{radial} = \frac{12EI}{L^3}$$

These cases are summarized in **Figure 30**. As in this case, both the model and experimental setup will not be allowed bit rotation, the latter expression was used to find the radial stiffness.

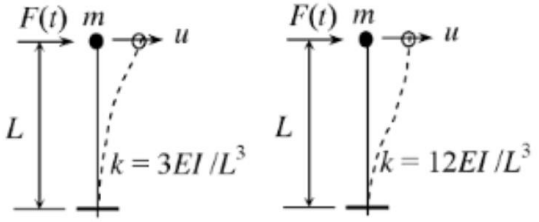

Figure 30. Different radial stiffness configurations.

Finally, the torsional stiffness was found using the following expression,

$$K_{tor} = \frac{GI_p}{L}$$

Where, G is the shear modulus and Ip is the polar moment of inertia.

The summary of the values assumed and resulting stiffness for each material can be observed in **Table 10**. As it can be seen a 6 ft in length rod was assumed to do this comparison.

It is with great deal of importance to note that the axial stiffness of steel exceeds more than double that of aluminum, 180 times that of PE and 100 times that of PVC. For radial stiffness, a similar trend of magnitude difference is observed. Finally, the torsional stiffness of steel is almost 30 times that of aluminum, around 6,600 times the one of PE and around 790 times that of PVC.

Table 10. Stiffness calculation comparison

Steel		**Aluminum**		**PE**		**PVC**	
OD (in)	*0.125*	OD (in)	*0.125*	OD (in)	*0.125*	OD (in)	*0.125*
OD(m)	*0.003175*	OD(m)	*0.003175*	OD(m)	*0.003175*	OD(m)	*0.003175*
E (Pa)	*2.00E+11*	E (Pa)	*7.10E+10*	E (Pa)	*1.10E+09*	E (Pa)	*2.00E+09*
G (Pa)	*7.93E+11*	G (Pa)	*2.70E+10*	G (Pa)	*1.20E+08*	G (Pa)	*1.00E+09*
A (m^2)	*7.92E-06*	A (m^2)	*7.92E-06*	A (m^2)	*7.92E-06*	A (m^2)	*7.92E-06*
L (m)	*1.82*	L (m)	*1.82*	L (m)	*1.82*	L (m)	*1.82*
Ip (m^3)	*9.98E-12*	Ip (m^3)	*9.98E-12*	Ip (m^3)	*9.98E-12*	Ip (m^3)	*9.98E-12*
I (m^4)	*4.99E-12*	I (m^4)	*4.99E-12*	I (m^4)	*4.99E-12*	I (m^4)	*4.99E-12*
Kaxial (N/m)	***870903.5***	**Kaxial (N/m)**	***309170.7***	**Kaxial (N/m)**	***4790***	**Kaxial (N/m)**	***8709***
Kradial (N/m)	***6.584***	**Kradial (N/m)**	***2.337***	**Kradial (N/m)**	***0.0362***	**Kradial (N/m)**	***0.0658***
Ktors (N/m)	***4.351***	**Ktors (N/m)**	***0.148***	**Ktors (N/m)**	***0.000658***	**Ktors (N/m)**	***0.00549***

The reason why this comparison is greatly important, it's to show that, as described in the introduction, the stiffness is the correlating factor between the loads applied to a system and the deflection response. Although there is a high difference between the stiffness of steel and aluminum, they are still comparable. However, when compared to the ones of PE and PVC, it can be seen that they are at least two orders of magnitudes apart which makes it impossible to compare deflections by applying the same loading conditions.

Although with dynamic analysis there are many factors involved in the type of results observed, it was determined that the stiffness was the main component responsible for this.

As such, a comparison between the steel and aluminum results are presented and discussed. The sets of results are related to the maximum deflection in the system, lateral deflections, axial deflections and torsional deflections.

The first step after performing a successful simulation was to determine the maximum total deformation over the time range. Then, the node where the maximum deflection was observed over the time range was picked and the total deformation of that node over time was retrieved and analyzed. It can be seen on **Figure 31** that all the configurations presented a similar pattern of vibration with the case of only displacements for aluminum being the highest, followed by the case of only displacements for steel, followed by the case of all modes for steel and finally the case of all modes for aluminum.

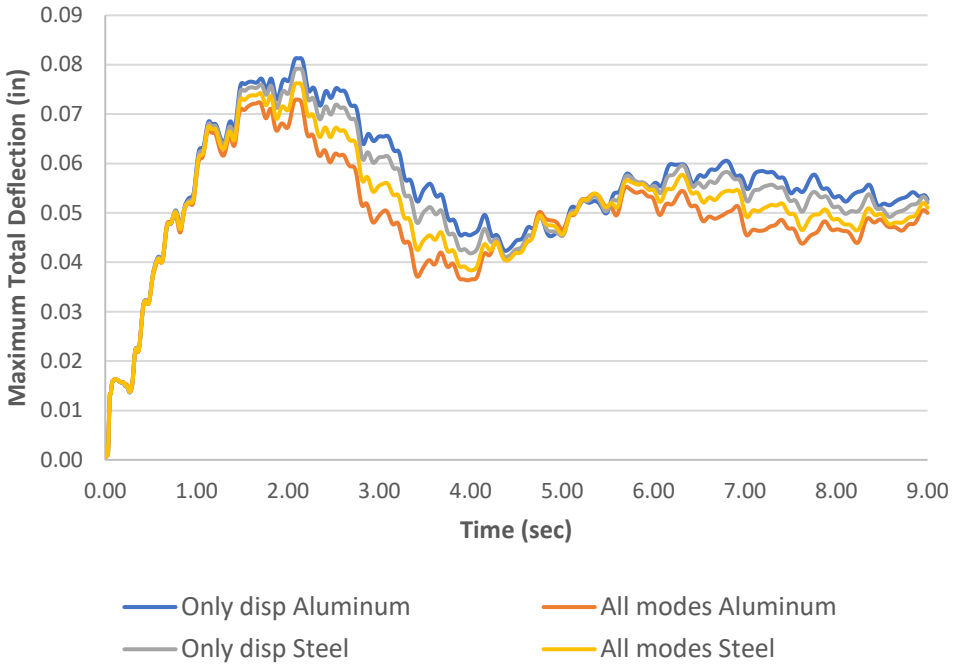

Figure 31. Point maximum deflection response.

Then on **Figure 32** it can be seen the results for lateral deflections. As observed, there is a lot of noise and clutter of data points which makes it impossible to analyze these results. Therefore, only the maximum peaks were filtered and retrieved and are shown in **Figure 33**. Once more, these are results which are still difficult to analyze properly which is why the average of these peaks were calculated and make up a single curve shown in **Figure 34**.

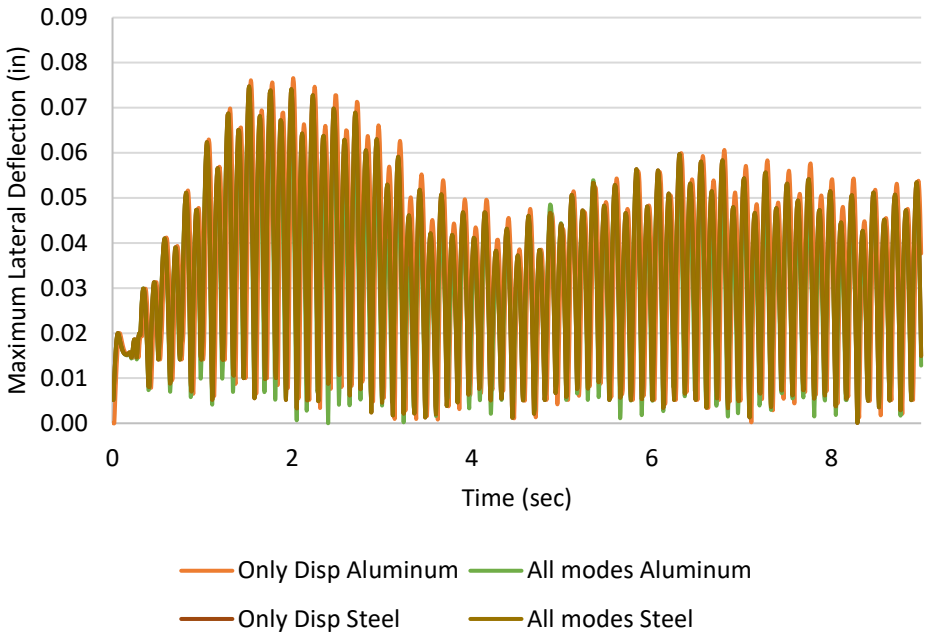

Figure 32. Raw results lateral deflections response.

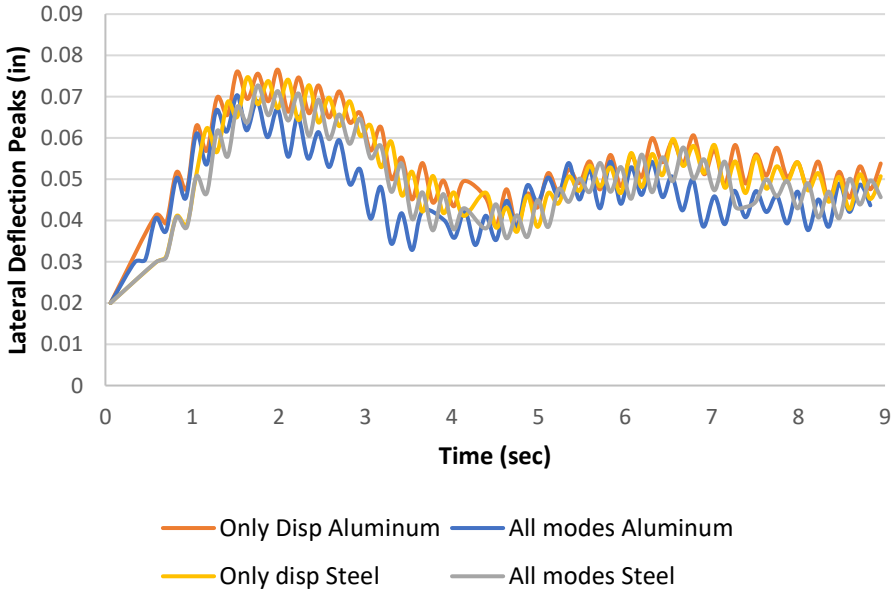

Figure 33. Filtered peaks for lateral deflection response.

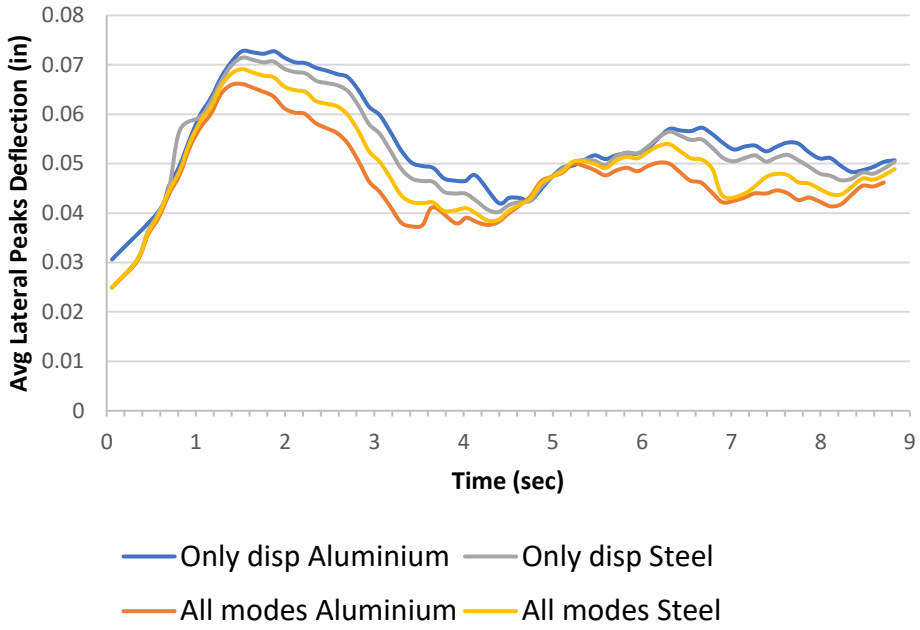

Figure 34. Averaged peaks for lateral deflection response.

Next, the axial deflections were obtained and can be seen in **Figure 35**. No modifications were made to this set of data.

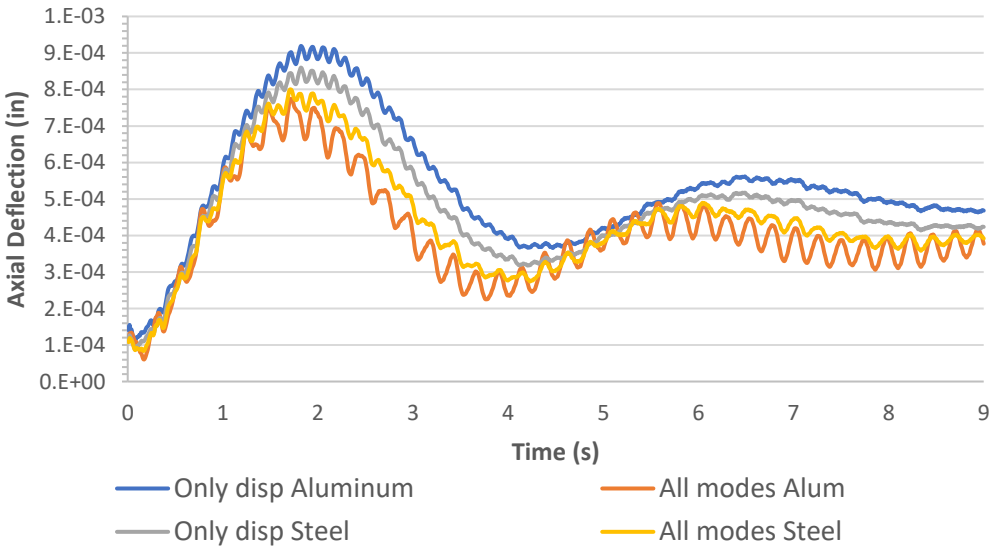

Figure 35. Axial deflections response.

Finally, the torsional deflection was obtained for the system. However, this data was obtained in inches with respect of a polar coordinate system located at the bit. This represents the arch length displaced with respect of the coordinate system. Therefore, given the radius of the rod and this arch, the deflection in degrees was calculated and is presented in **Figure 36**.

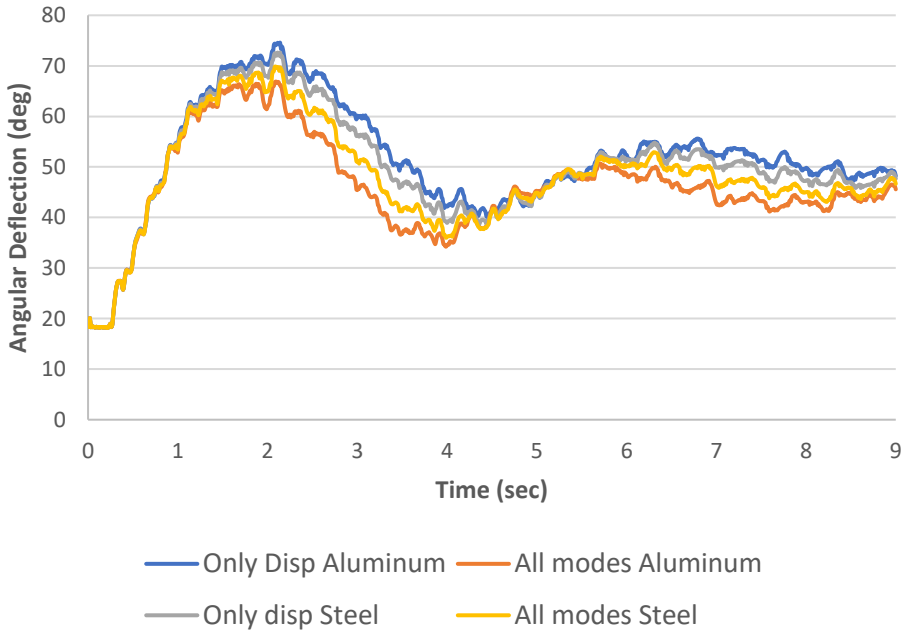

Figure 36. Torsional deflection response.

In order to compare these results appropriately, the damping coefficient (ξ), period of oscillation, and frequency were calculated and compared. The summary of the resulting values can be observed in **Table 11**. As it can be seen, for almost all cases with the exception of axial deflections, when one mode of vibration is induced, the aluminum has a higher damping coefficient than the steel, and the steel has a higher vibration frequency response than the aluminum. This can be explained from the damping ratio, which can be expressed as follows (Rao 2007),

$$\xi = \frac{C}{C_{cr}} = \frac{C}{2\sqrt{KM}}$$

Where C is the damping coefficient, C_{cr} is the critical damping coefficient, K is the stiffness coefficient and M is the mass coefficient in the equation of motion presented earlier.

As it can be seen from this formula, the damping ratio its inversely proportional to the stiffness and mass of the system. Therefore, it is expected that when applied one mode of vibration, the system with a lower stiffness and mass will present the lowest damping ratio.

The behavior of the steel having a higher vibration response frequency can be explained using the natural frequency expression (Rao 2007),

$$\omega_d = \sqrt{1 - \xi^2}\omega_n$$

Where, ω_d is the frequency of the damped vibration and ω_n is the natural frequency. From this expression, it can be seen that the frequency response its directly proportional to the difference between one and the squared of the damping ratio. This means that the higher the damping ratio is, the lower the frequency response will be when a single vibration mode is applied and vice versa. Therefore, given than the damping ratio of the aluminum is higher for most cases when a single mode of vibration is applied, then the frequency response will be lower than the steel's response.

However, when all modes of vibration are present, for almost all cases, the steel will have a higher damping coefficient whereas the aluminum will have a higher frequency of vibration response.

A special case is observed for the axial deflection case where, in the case of only one mode of vibration, the steel has a higher damping coefficient and both aluminum and steel present the same vibration response frequency.

Table 11. Simulation results comparison.

	Aluminum				Steel				Summary	
Case	**ξ**	**Period (s)**	**Frequency (Hz)**	**Frequency (rad/s)**	**ξ**	**Period (s)**	**Frequency (Hz)**	**Frequency (rad/s)**	**ξ**	**Frequency**
Maximum Deflection Only Displacement	*0.0469*	*4.71*	*0.212*	*1.333*	*0.0452*	*4.19*	*0.239*	*1.499*	Aluminum is higher	Steel is higher
Total Deformation All Modes	*0.0442*	*3.61*	*0.277*	*1.740*	*0.0444*	*4.21*	*0.238*	*1.492*	Steel is higher	Aluminum is higher
Lateral Def Only Displacement	*0.0381*	*5.15*	*0.194*	*1.219*	*0.0375*	*4.79*	*0.209*	*1.311*	Aluminum is higher	Steel is higher
Lateral Def All Modes	*0.0438*	*4.67*	*0.214*	*1.345*	*0.0395*	*4.79*	*0.209*	*1.311*	Aluminum is higher	Aluminum is higher
Axial Def Only Displacement	*0.0783*	*4.67*	*0.214*	*1.345*	*0.0808*	*4.67*	*0.214*	*1.345*	Steel is higher	Both are the same
Axial Def All Modes	*0.0733*	*3.86*	*0.259*	*1.627*	*0.0783*	*4.33*	*0.231*	*1.450*	Steel is higher	Aluminum is higher
Torsional Def Only Displacement	*0.0467*	*4.65*	*0.215*	*1.351*	*0.0449*	*4.17*	*0.240*	*1.506*	Aluminum is higher	Steel is higher
Torsional Def All Modes	*0.0442*	*3.62*	*0.276*	*1.735*	*0.0443*	*4.21*	*0.238*	*1.492*	Steel is higher	Aluminum is higher

A very interesting and significant behavior is observed when all modes of vibration are induced in the system. For most cases, with the singular exception of the lateral deflection, the behavior of the damping ratio and frequency response is flipped. Meaning, for all except for lateral deflections, the steel will perceive a higher damping ratio than the aluminum and the aluminum will perceive a higher frequency response. The only exception is the lateral deflection response where the aluminum has both a higher damping ratio and frequency response.

A possible explanation for this behavior is related to the coupling of all three modes of vibration. When only one mode of vibration is induced in the system, the system reacts in a predictable manner given the known equations for one mode of vibration which are related to the stiffness of the materials. However, when more than one mode of vibration is present, the displacements occurring are a reaction to more than one mode at the time. For example, axial vibration makes the string shorter and longer throughout its application. Torsional vibration also will shorten and elongate the string as it twists the pipe. How these two interact with each other causes the string to behave in a different way than predicted due to the previously presented equations. Further analytical analysis is required to fully describe the behavior of the system to explain this change in behavior. It is because of these observations that it is highly recommended when studying drill-string vibrations to include all modes of vibration. Otherwise, the behavior and response of the system may vary in unpredictable ways.

Finally, comparing the general reactions of the system when one mode of vibration is induced against all modes of vibration being applied, a clear difference is observed. When all the modes of vibration are applied to the system, the overall deflection for any of the

cases observed, will be lower than for the case with only one mode of vibration being applied.

This can be explained due to the distribution of mechanical energy in the system. As it was explained in the introduction, mechanical vibrations are characteristic of the mechanical energy distribution of the system when a disturbance is introduced. As it can be clearly seen from **Figures 31-36**, the amplitude of the vibrations is higher than when only one modes is induced. This is because the mechanical energy is distributed among the different responses occurring simultaneously due to disturbances occurring in the lateral, axial and torsional directions.

This phenomenon corroborates what was observed in the previous presented study. A possible way to mitigate drill-string vibrations is to induce other modes of vibration in a control manner. This could mitigate the response of the vibration response to acceptable and controllable values.

Additionally, a very similar conclusion was presented out of an extensive study made by NOV where they researched the effects that inducing axial vibrations have on ROP and stick-slip. They found that inducing axial vibrations reduces significantly bit RPM variation (stick-slip) and increases significantly ROP (Clausen 2014). This extensive study supports the same idea made in this thesis that, by inducing controlled vibrations, the vibration response in the system will be lower.

3.2.8 Conclusion

After performing this study, several conclusions were reached:

- The stiffness of the four studied materials was calculated and compared.
- Due to the significant difference in magnitude of the radial, axial and torsional stiffness, the materials polyethylene and polyvinyl chloride had to be excluded from the modelling.
- Successful vibration simulation was made for structural steel and aluminum for two main configurations: inducing one mode of vibration and inducing all three modes.
- It was compared and analyzed the vibration response for steel and aluminum for four different cases: maximum deflection response, lateral deflection response, axial deflection response and torsional deflection response.
- It was observed that for most cases, when one mode of vibration is induced, the aluminum will have a higher damping ratio than the steel and the steel will have a higher frequency response than the aluminum. The only exception was the axial deflection response where the steel had a higher damping ratio and both the aluminum and steel had the same frequency response.
- It was observed that when all the modes of vibration were applied to the system, for most cases, the steel will have a higher damping ratio and the aluminum will have a higher frequency response. The only exception was seen for the lateral deflection response where aluminum had a higher damping ratio.
- It was determined comparing the two major cases studied that, when only one mode of vibration is induced, the vibration response will be higher than when all

three modes are applied. This corroborates what was presented in the previous study (Marquez, Omojuwa and Teodoriu 2017), and leads to the possibility of mitigating downhole vibrations by inducing different controlled modes of vibration.

3.2.9 Recommendations for future studies

It is highly recommended that this study is taken as a step toward the development of a method to mitigate downhole vibrations using other controlled modes of vibration. It is recommended to study the effect that inducing vibrations at different frequencies will have on the vibration response. Another extension to this study will be comparing the vibration response by having stabilizers placed in different positions in the drill-string and comparing with having no stabilizer. For calibration and validation purposes, it is highly recommended to compare results with experimental setup testing. Finally, the expansion of this study to different materials is recommended.

Chapter 4: Downscaling for New Experimental Setup

4.1 Methodology

Before presenting the mechanical design of the new setup, the downscaling steps taken of both geometrical and mechanical parameters will be discussed in this section.

4.1.1 Application of Law of Similitude

Law of similitude (or Similarity Theory) allows researchers to take information, seen in real life, and create a model in a laboratory downscaling geometrical cinematic and dynamic parameters. The considerable challenge of downscaling a drill-string, is the fact that they real drill-strings can be in length thousands of feet in length, and when linearly geometrically downscaled, the dimensions of the pipe needed to recreate the same factors such as stiffness and inertia, become nearly impossible. Moreover, if a pipe or rod is found with the proper downscaled geometrical parameters, the dynamic parameters might not be practical to recreate. That is why in some of the few downscaled available models, the process of using different string material becomes crucial.

As the objective of the proposed setup is to represent both geometrically and dynamically what could be seen in the field, three critical parameters were considered for the scaling of the model.

1. Angular deflection
2. Critical buckling force
3. Torque and power required

To find these parameters for the model, the first step is to find the downscaling factor for the geometry.

4.1.2 Downscaling Factor

The general first step to find the *downscaling factor* is, given a well geometry, the measured depth can be obtained, and by dividing by the laboratory resulting measured depth, the downscaling factor 'n' is obtained as follows,

$$n = \frac{MDlab}{MD}$$

Where,

$MDlab =$ Laboratory measure length (ft)

$MD =$ Measured depth (ft)

For the vertical configuration, the expression will result as follows,

$$n = \frac{TVDlab}{TVD}$$

Where,

$TVDlab =$ Laboratory vertical length (ft)

$TVD =$ True Vertical Depth (ft)

The problem with this approach is that when a 'n' value is obtained and it is used to downscale the OD of a typical 5" drill-pipe, the resulting model outside diameter yields unpractical values that cannot be found by any manufacturer to the best of the author's knowledge. Therefore, a fixed OD of the smallest rod of several materials that can be found is used together with the OD of the typical drill-pipe to find the value of 'n'. The expression to find the downscaling factor is as follows,

$$n = \frac{OD_{model}}{OD_{drillpipe}}$$

Where,

$OD_{model} =$ Smallest available outside diameter that can be found for different materials (in)

$OD_{drillpipe}$ = Typical value of outside diameter for a drill-pipe (in)

Knowing now our downscaling factor and the laboratory space available for the model, an 'upscaling' of the setup is made to determine what will be the TVD that the setup will be able to represent.

4.1.3 Shear modulus and maximum torque

Next, is to find the required torque for the model. As a major interest of this study is to create a setup that will generate torsional vibrations such as stick-slip, a proper downscaled torque is needed. To derive the expression used to calculate the downscaled torque, it was started from the torque formula expressed as follows,

$$Torque = \frac{\tau J}{R}$$

Where,

τ: Shear stress (psi)

J: Polar moment of inertia of an area (in^4)

R: Distance from the center to stressed surface in the given position (in)

Next, knowing that the polar moment of inertia is expressed as,

$$J = \frac{\pi}{4}(OD^4 - ID^4)$$

Where,

OD: Outer diameter of the cylinder or pipe (in)
ID: Inner diameter of the cylinder or pipe (in)

Then, solving for the shear rate and equating both the real and downscaled expressions, we get the following expression for the downscaled torque,

$$T_{model} = \frac{T_{real}}{n}\frac{G_{model}}{G_{real}}\left(\frac{od^4 - id^4}{OD^4 - ID^4}\right)$$

Where,

T_{model}: Torque needed in the model (lbf ft)
T_{real}: Torque applied in the real case scenario (lbf ft)
G_{model}: Shear modulus of the model's material (psi)
G_{real}: Shear modulus of the real case material (steel) (psi)

4.1.4 Weight on Bit

There are two critical forces that need to be downscaled for the model. First, is the weight-on-bit (WOB) force, and second are the lateral forces that induce whirling.

To downscale the WOB, a fixed value of WOB was chosen of 5 tons. Then, using Newton's 2nd law and assuming that both the real and downscaled model have the same acceleration, the following expression was used to find the require downscaled WOB,

$$F_{real} = M_{real}\, a = M_{ds} a = F_{ds}$$

$$F_{ds} = 2000 * WOB * n \frac{(od^2 - id^2)}{(OD^2 - ID^2)} \frac{\rho_{ds}}{\rho_r}$$

Where,

$WOB =$ Weight on bit (tons)
$n =$ Downscaling factor
$od =$ Downscaled outside diameter (in)
$id =$ Downscaled inside diameter (in)
$OD =$ Outside diameter (in)
$ID =$ Inside diameter (in)
$\rho_{ds} =$ Density of the selected material (lb/in^3)
$\rho_r =$ Density of steel (lb/in^3)

Then, to know the maximum WOB that can be applied to the model without creating buckling, the critical buckling force was calculated using the following equation,

$$F_{cr} = 2\left(\frac{EIW sin\theta}{r}\right)^{1/2}$$

Where,

$E =$ Young modulus (psi)
$I =$ Axial moment of inertia (in^4)
$W =$ Weight per unit length (lb/in)
$\theta =$ Inclination
$r =$ Radial clearance (in)

4.1.5 Lateral Forces

To recreate whirling and lateral vibrations, displacements instead of forces will be induced in the system. In the simulations in the previous sections, a sinusoidal displacement disturbance was applied at the bit at a certain frequency and a fixed maximum magnitude of deflection. Given that the experimental setup will include a high frequency movement generator (hexapod), this will stay consistent for the study and future comparison of the simulation model. The use and description of this device will be presented in a future section.

4.1.6 Power Equivalent

To properly select the configuration of the motor for the model, the power equivalent to rotate the drill-string at a constant angular velocity of 250 rpm was calculated with the following expression,

$$P = 1.3558 * T\omega$$

Where,

$P =$ Power (Watts)
$T =$ Torque (lbf ft)
$\omega = \frac{2\pi}{60} rpm$

Chapter 5: CAD Design of Experimental Setup

5.1 Experimental setup components

In order to create a physical model with such a high degree of complexity, a CAD model using the commercial software SolidWorks was used. The designing phase was conducted in four parts:

1. Laboratory Structure
2. Top Drive Assembly
3. Bottom Assembly
4. Drill-string

5.1.1 Laboratory Structure

The laboratory space provided by the University of Oklahoma to conduct this experiment was simplified and modelled in a CAD model to get a better representation of the dimensions and orientation that the different equipment will have once the setup is build. The bounding space of the laboratory was first measured and can be seen in **Figure 37** with a 9.875 ft x 9.875 ft x 47.5 ft space.

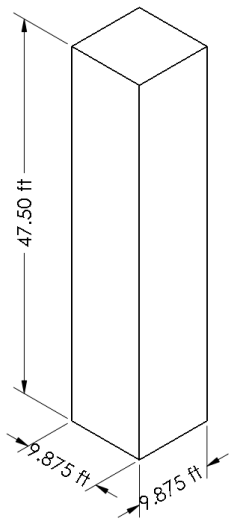

Figure 37. Laboratory space schematic.

Then, the structure was designed with beam columns, pattered steel floors and concrete walls. A latter and the relative positioning of the hole was also included in the design of the structure for visual scaling and reference. The final product can be seen in **Figure 38**.

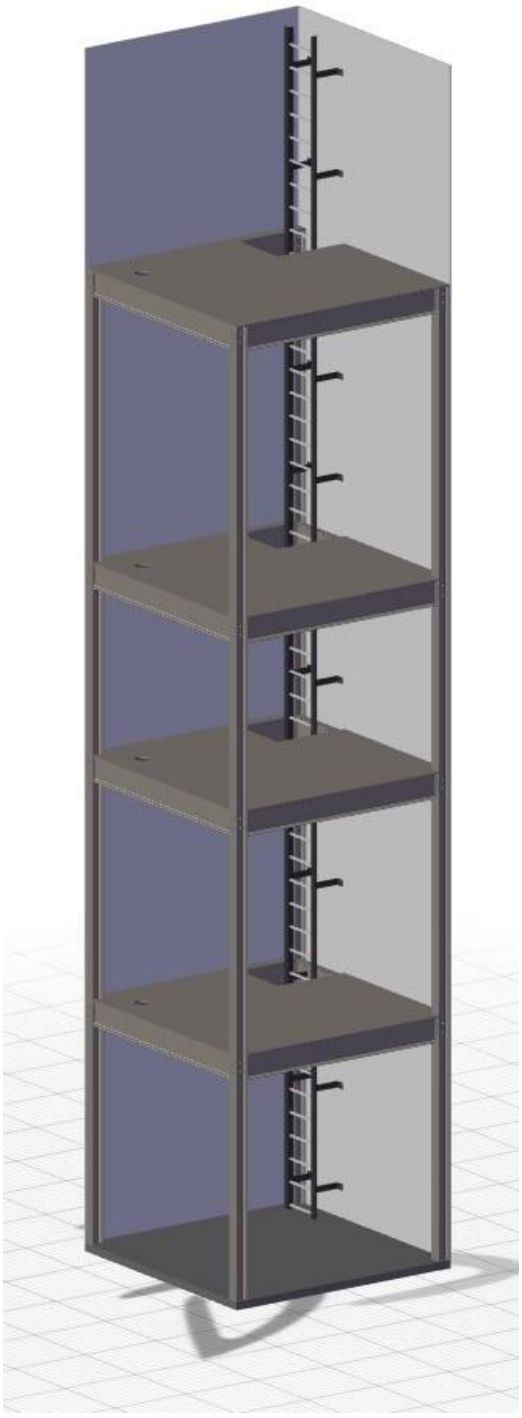

Figure 38. CAD model of laboratory space structure

5.1.2 Top Assembly

The top assembly of the experimental setup needed to recreate the same functions as a drilling rig. That is, it needed to have a top drive that generates the RPM and provides torque to the drill-string. It also requires a hoisting system that will control the weight-on-bit. The assembly of the setup's top drive is shown in **Figure 39**. The RPM generator is the motor of an 18 V hand drill that functions with DC current. Its voltage will be controlled via a digital power supply. Then, the WOB representing the hoisting capabilities of the system is made by the combination of a translocator and a stepper motor which will control the hoisting and lowering of the string at a wide but precise range of speeds. The top drive rests on top of a 'XY controller' which moves the string in any coordinate within a certain range in the perpendicular plane. Finally, as shown in **Figure 39** as well, the setup includes three sensors that will show the main parameters controlled by the drilling engineer which are WOB, Torque and RPM.

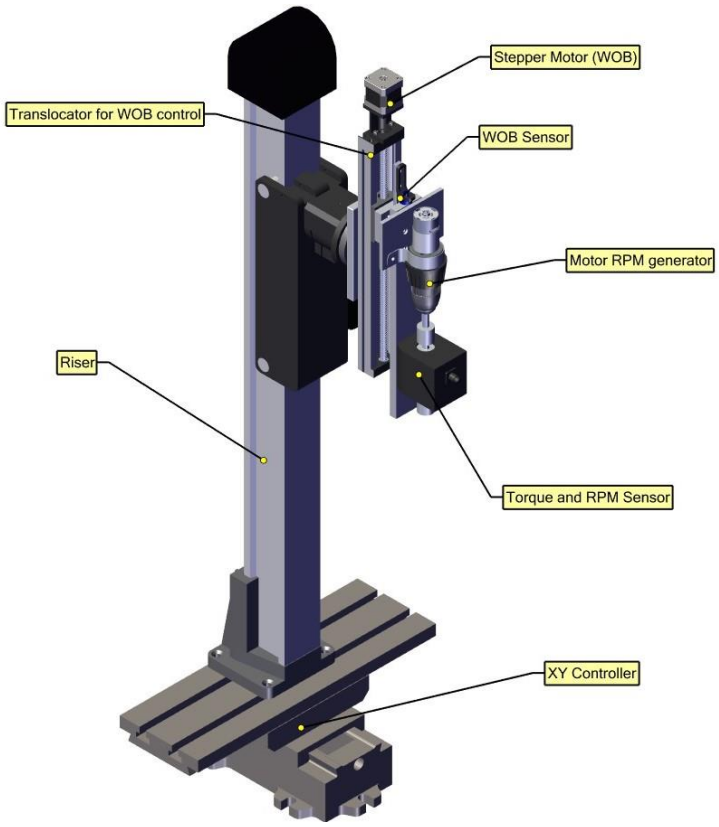

Figure 39. Top assembly CAD model and breakdown.

5.1.3 Bottom Assembly

The bottom assembly needed to account for several factors that are present in the field. The final assembly for the vertical configuration of the setup can be seen in **Figure 40**. First, it had to recreate and control the desired ROP. For that, the main unit (hexapod, sensors and break) was mounted on a wide and solid aluminum plate that in turn is mounted on top of two rails as it can be seen in **Figure 41**. The movement of this plate is controlled by a similar devise presented in the latter section of the top drive, which is controlled by a stepper motor. Then, to recreate any type of vibration and bit rock interaction, two main components are used. The first is the electro-magnetic break (EM Break) which will be the responsible for generating the stick-slip condition. Second, it's

the hexapod or high-frequency movement generator. This devise can move with 6 degrees of freedom and has a strut resolution of 50 nano meters. It can move with up to 4g of acceleration and a 250 mm/s speed. We expect that this devise will be able to reproduce the most severe bit-rock interaction processes. Both of these devises are labelled in **Figure 40**. Finally, as a way to control the forces impacting the bit of the drill-string, a force sensor was installed between the movement platform of the hexapod and the electro-magnetic break.

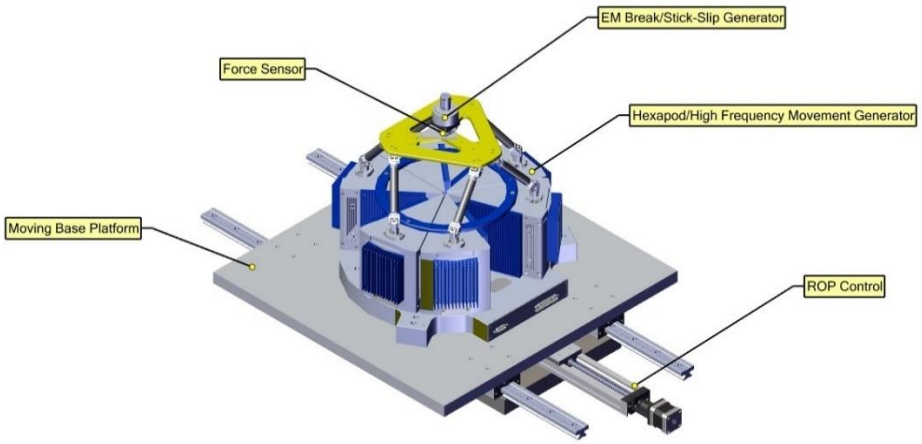

Figure 40. Bottom assembly CAD model and breakdown.

5.1.4 Drill-string

The drill-string recommended for this devise is a 1/8" OD aluminum rod. The reason for the size of the pipe is related to the fact that, when geometrical downscaling is performed, if it is desired to analyze the largest possible length of real drill-string on the field, then the smallest dimensions for the selected material needs to be used. This will allow to recreate around 1,900 ft of pipe which is larger than any other setup up to date. As a reference, it can be seen in **Figure 41** that this setup will be the largest downscaled

vibration model by far. The distances in this figure are in meters. This fact will allow to address the size limitation that is commonly observed in other experimental setups.

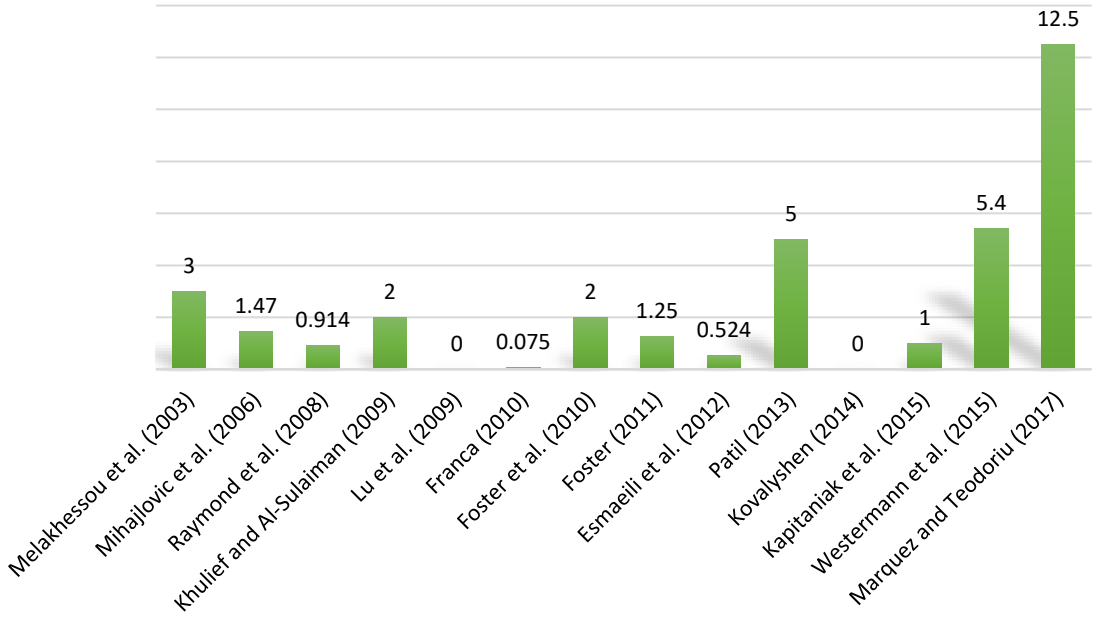

Figure 41. Size comparison of the available experimental setups in comparison with the presented one.

The recommended material for this rod is aluminum. The reason for this is due to the results of the simulated studies previously presented. Only two materials were able to be studied and compared, structural steel and aluminum. Aluminum is expected to allow a better representation of what is observed in the field due to having lower stiffness. Moreover, if an experiment with an aluminum rod is performed under the same or similar conditions as the simulation presented in section 3.2, then this model could prove to be valid and extended to predict a more accurate representation of reality. Other materials can be used as well and a comparison of the behavior of the stiffness can be obtained and compared with the simulation results.

What is important is that this setup is design to accommodate any type of string material as long as it has the same geometrical parameters.

5.2 Setup Model Assembly

After all of these different sub-assemblies were designed, two configurations of the final setup assembly were made. As mentioned earlier, the purpose of this setup is to be able to recreate different well geometries. For that purpose, two configurations were designed and are presented in this work, a vertical and a horizontal well configuration.

5.5.1 Vertical Configuration

The main configuration which will be at the center of the first phase of experimental studies is the vertical configuration. This is because it is needed first to compare to other experimental setups presented in a previous section as well as with Finite Element models made by the author of this work. The vertical configuration assembly can be seen in **Figure 42**.

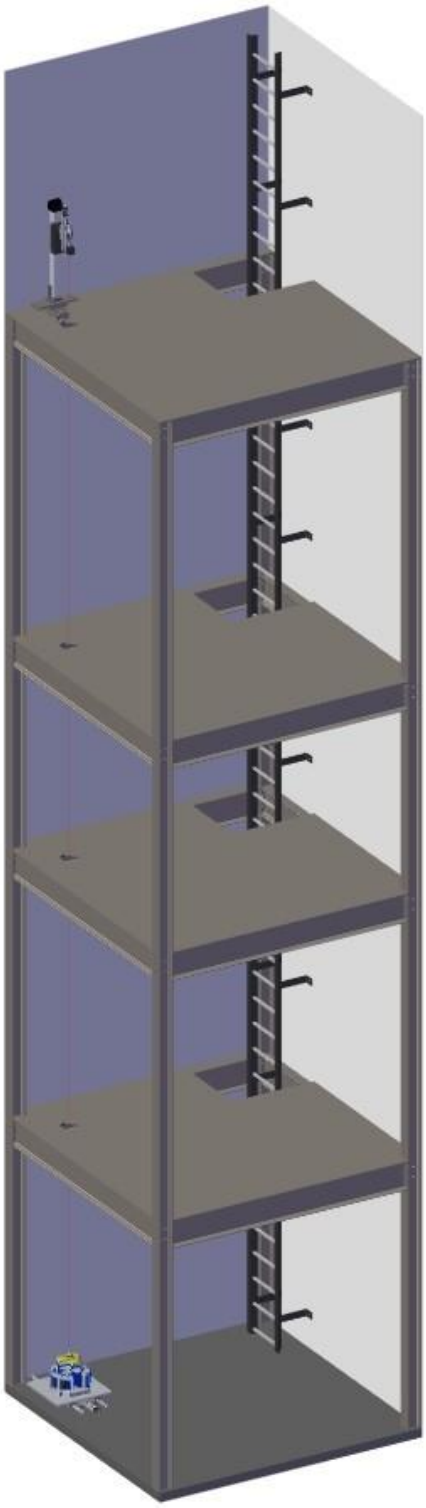

Figure 42. Vertical configuration of experimental setup.

5.2.2 Horizontal Configuration

To provide an example of the different geometries that could be achieved with this experimental setup, a horizontal well with a medium curvature ratio was designed and is presented in **Figure 43**. Although this configuration was not tested, the components and connections should not change considerably as the sub-assemblies would remain the same. Only the pipe and the annulus will change as well as the direction the EM break and pipe are connected. For a better representation of the pipe and bottom assembly positioning **Figure 44** is also presented.

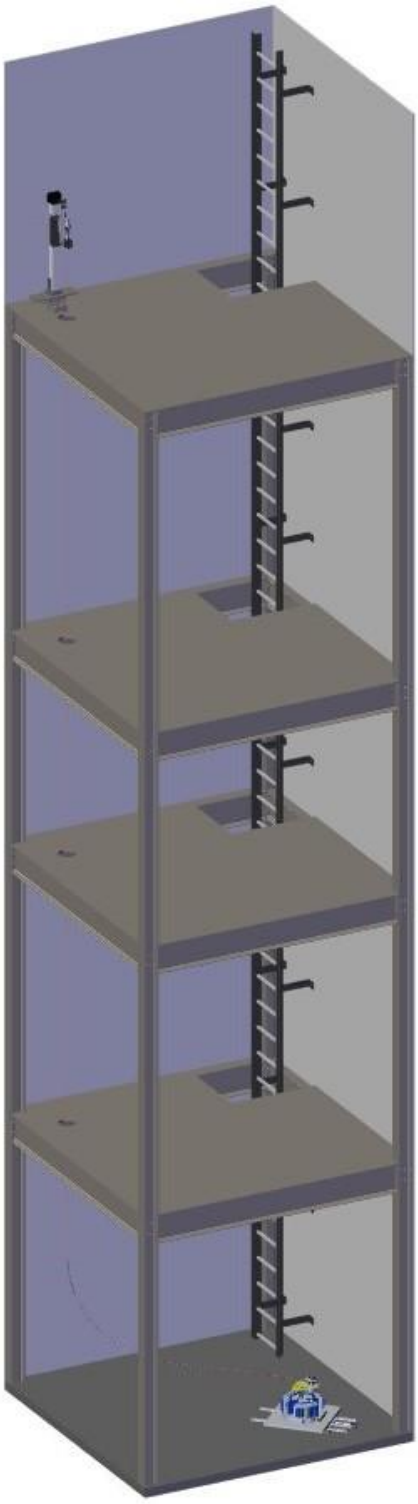

Figure 43. Horizontal configuration of experimental setup.

Figure 44. Side view of horizontal configuration experimental setup.

Chapter 6: Experimental Setup

After the design, manufacturing and acquisition of the different required components, these were put together to create the new presented experimental setup for drill-string vibrations at the Sarkeys Energy Center at the University of Oklahoma.

6.1 Bottom Hole Assembly

The final assembled setup of the bottom hole assembly of the new experimental setup can be seen in **Figure 45**. There are 7 main components in this setup which matches closely what was planned and designed. First, number 1 in this figure, the hexapod can be seen. The enclosed caged is for protection of the hexapod and it is recommended by the manufacturer to keep it on until the hexapod is in operation.

The hexapod is mounted on top of an aluminum plate, marked with number 2. This plate provides a solid base for the hexapod, and a safe and secure connection with the rails guides (number 3) and rails (number 4). The axial movement of the hexapod is controlled by a stepper motor connected with a gear box to provide the necessary torque (number 5). This axial movement will be used in the horizontal configuration of the setup. The motors are connected to the ROP control (number 5). To provide stability and absorb any undesired vibration of the setup, a steel plate is the base for this entire bottom hole assembly setup (number 6). Finally, the electromagnetic motor discussed in the previous section is connected to the hexapod's platform (number 7). This motor will be used to induce torsional vibrations. A more detailed view of the components, number 2-7 are shown in **Figure 46**.

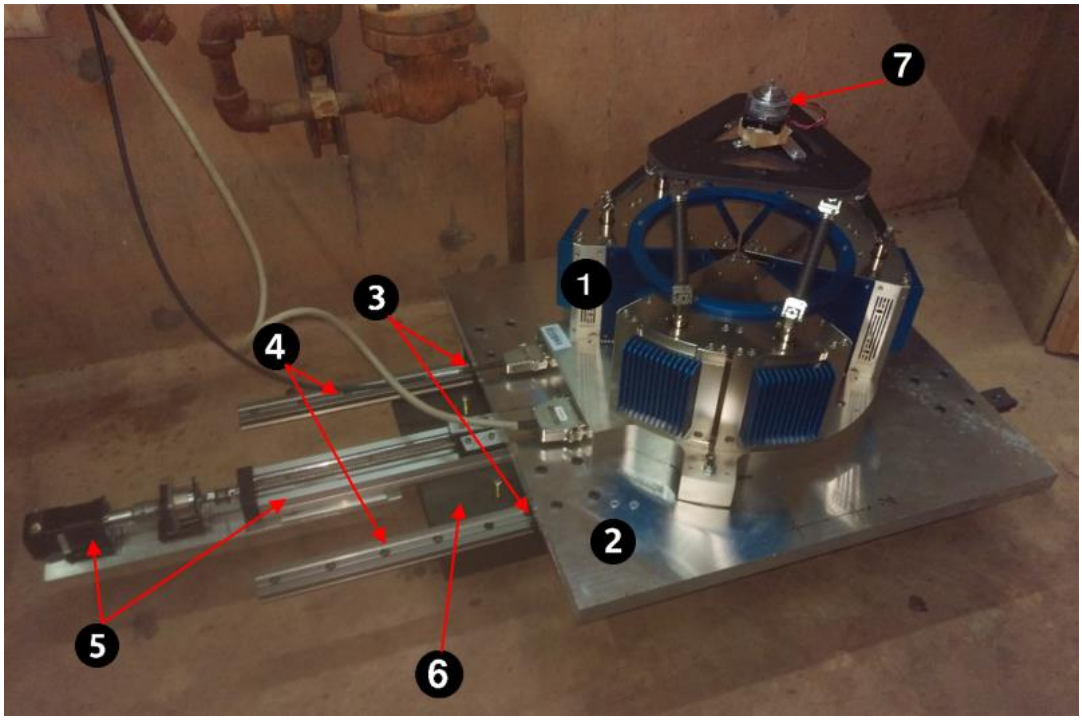

Figure 45. Bottom Hole Assembly finished setup.

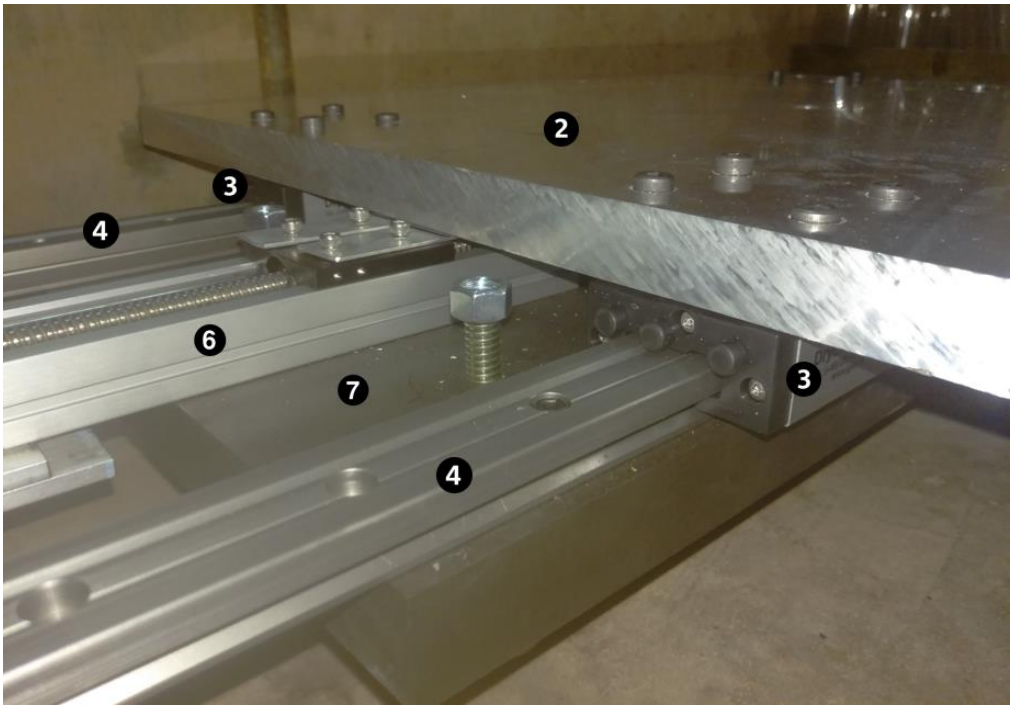

Figure 46. Detailed view of BHA finished setup.

6.2 Top Assembly

The final configuration for the top assembly of the new experimental setup can be seen in **Figure 47**. There are also 7 main components in the top assembly and are numbered 1-7 in this figure as well. Number 1 is the riser devise which will allow the entire structure be raised and secured at a vertical location. Then, to orient the string in the perpendicular plane, an XY displacer was used (number 2). This will allow the setup to be positioned in different positions. The motor in charge of applying the WOB and also any extra vertical movement that the string requires, similar to the bottom hole assembly, are shown with numbers 3 and 4. Then, a WOB sensor was placed in the connection between the vertical displacer and the motor (number 5). The main source of rotation and torque will be provided by the motor of a manual drill (number 6). This allows for different torque configurations just as a regular drill. Finally, to monitor the torque applied on the string a torque sensor was attached to the motor via a metal link (number 7).

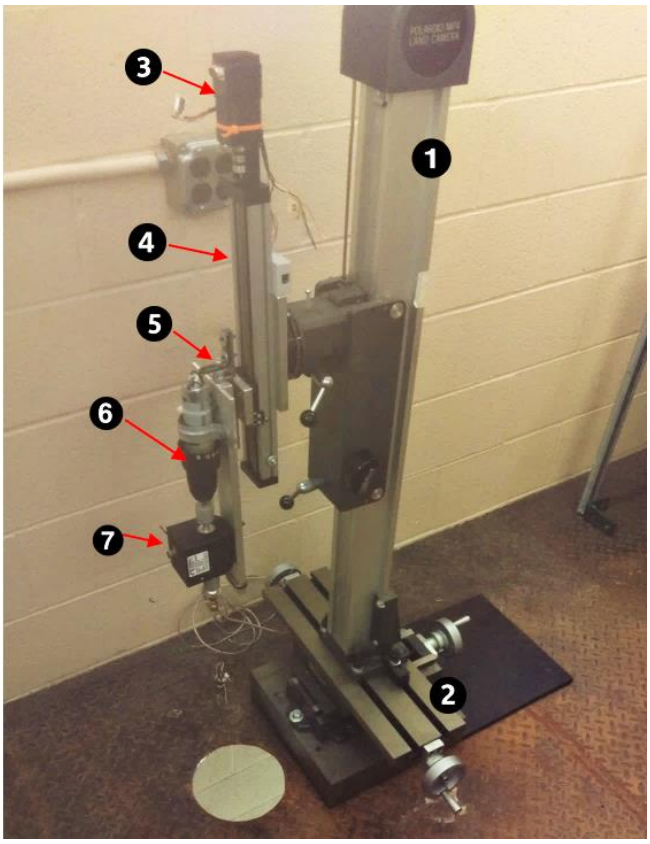

Figure 47. Top assembly finished setup.

6.2 String and future components.

Although, most of the necessary components are ready and assembled in the way it was designed, there are some components that are highly recommended to be included.

First, it is recommended that different materials of string are tested. As it was presented in the Finite Element models, it is highly beneficial to study the behavior of different materials in the setup. Particularly, steel, aluminum and PVC are recommended initially. However, based on the simulations presented, aluminum will be the most beneficial initially to combine with the FEA model. That way, the model can be calibrated and expanded to test different materials and well configurations. Later, other strings can be

tested and compared with the simulation, providing an insightful behavior to analyze and study vibrations.

The limitation that was presented during this study is the unavailability of rod or pipe strings with the designed dimensions of these different materials.

An extension of this study can also include the placement of stabilizers as the finite element models do.

Several components are missing at the moment of the presentation of this work that are highly recommended to be included in the testing stage. The most important component that is necessary is an RPM sensor both at the top and the bottom assembly. Without the careful monitoring of this parameter, any analysis on how the drilling parameters can affect and mitigate downhole vibrations will be incomplete.

Another critical piece of equipment that it is highly recommended to be included in the testing stage is accelerometers. Accelerometers are used to measure vibrations and cen be attached in different sections of the string, including the bit, the top and sections at the middle.

Finally, another critical equipment that at the moment of presenting this work could not be acquire is a force measuring device for the bottom assembly. This force measuring device will be connected to the EM break and will be the link between the top hexapod platform and the string. With this device, it will be possible to measure process in the three axes of movement, including the WOB.

Chapter 7: Conclusions and future work

In this study, an extensive review of current research related to drill-string vibration was presented focused on three areas: analytical work, finite element models, and experimental setups. It was analyzed the limitations that current experimental setups have and how they can be addressed.

Two detailed finite element studies are presented. Both tackled an unprecedented issue of coupling the three modes of vibration into a single model. The first, studied and compared the BHA dynamic reaction when one mode of vibration was applied versus the three modes of axial, lateral and torsional were induced in the system. The effects of changing the magnitudes of those vibration was also presented and discussed. It was discussed the importance of stabilizer use in bottom hole assemblies in order to mitigate significantly vibration propagation. It was concluded as well that when only one mode of vibration is applied, the magnitude of the vibration response is considerably higher than when all modes are present. This inspired one of the objectives of the second presented study.

The second study expanded the scope of the first one and had the objective to compare four different materials (steel, aluminum, PE and PVC) when one mode was induced versus when all three modes where applied. A modal analysis was also studied and the stiffnesses of the different materials were calculated and compared. It was concluded from these studies that when all modes of vibration are present, the vibration response decreases due to the mechanical energy redistribution. It was also concluded that when one mode of vibration is applied, the behavior of the system can be predicted based on known equations, whereas when all the modes are induced the dynamic behavior of the

system changes considerably to where it does not longer follow the same equations and predictable behavior.

These results lead to the possibility of mitigating downhole vibrations by inducing other controlled vibrations. If one particular mode of vibration is being particularly detrimental to the drilling operation, inducing another controlled vibration might reduce the magnitude of the harmful vibration to manageable levels. Experimental work needs to be done in order to corroborate this model.

An experimental setup was designed with downscaled parameters that will allow to corroborate or calibrate better these simulated models. This experimental setup will address most of the issues that others haven't been able to address, specially the size limitation. With a designed length of 41 ft vertical and the possibility of having a horizontal section of up to 8 ft, this will be the first setup able to recreate up to 1900 ft of drill-string as well as comparing the behavior between vertical and vertical with horizontal sections. The setup was designed to accommodate any type of drill-string material but it is recommended the use of 1/8" OD aluminum pipe in order to observe comparable results with the simulation.

The use of this setup as recommended will allow for the acquisition of important simulation calibration information such as the damping vs frequency table, which can be used as an input in the finite element model to acquire more accurate results. Once the model is calibrated and corroborated, it will be possible to simulate different materials and well geometries as well as study the effect of different stabilizer placement.

In the near future, once the proposed experimental setup is tested successfully, an innovative Hardware-In-Loop will be implemented in this setup. With the

implementation of a HIL, a software can be programmed to recreate vibration situations that occur in the field, and the same software will be able to modify the operational parameters of WOB, RPM and TOB in a way that it will reduce the possibility of encountering harmful vibrations.

The overall conclusion of this work is to contribute to the already extensive research work to show the importance of studying the drill-string dynamics in order to mitigate vibrations to successfully drill the intended well in a safe, cost effective and environmental safe manner.

References

Ashley, D.K., X.M. McNary, and J.C. Tomlinson. 2001. "Extending BHA Life with Multi-Axis Vibration Measurements." *SPE/IADC Drilling Conference.* Amsterdam, The Netherlands: SPE/IADC.

Axisa, F., and J. Antunes. 1992. "Flexural Vibrations of Rotors Immersed in Dense Fluids Part I: Theory." *Journal of Fluids and Structures* 3-21.

Berlioz, A., and J. Der Hagopian. 1996. "Dynamic Behavior of a Drill-String: Experimental Investigation of Lateral Instabilities." *Journal of Vibration and Acoustics 118* 292-298.

Clausen, J.R., Schen, A.R., Foster, I., Prill, J., Gee, R. 2014. "Drilling with Induced Vibrations Improves ROP and Mitigates Stick-Slip in Vertical and Directional Wells." *2014 IADC/SPE Drilling Conference and Exhibition.* Forth Worth, TX: SPE/IADC.

Darein, D. W., and B. J. Livesay. 1968. "Longitudinal and Angular Drillstring Vibrations with Damping." *Journal of Engineering for Industry* 671-679.

Esmaeili, A., B. Elahifar, R. K. Fruhwirth, and G. Thonhauser. 2012. "Laboratory Scale Control of Drilling Parameters to Enhance Rate of Penetration and Reduce Drill String Vibration." *SPE Saudi Arabia Section Technical Symposium and Exhibition.* Al-Khobar, Saudi Arabia: Society of Petroleum Engineers.

Foster, I., A. Macfarlane, and R. Dinnie. 2010. "Asymmetric Vibration Damping Tool - Small Scale Rig Testing and Full Scale Field Testing." *2010 IADC/SPE Drilling conference and Exhibition.* New Orelans, LA, USA: IADC/SPE.

Franca, Luiz F. P. 2010. "Drilling Action of Roller-Cone Bits: Modeling and Experimental Validation." *Journal of Energy Resources Technology 132* 1-9.

Kapitaniak, Marcin, Vahid V Hamaneh, Joseph Paez Chavez, Krishnan Nandakumar, and Marian Wiercigroch. 2015. "Unveiling complexity of drill-string vibrations: Experiments and modelling." *International Journal of Mechanical Sciences* 324-337.

Kovalyshen, Y. 2014. "Experiments on Stick-Slip Vibrations in Drilling with Drag Bits." *US Rock Mechanics / Geomechanics Symposium.* Minneaplis, MN, USA: ARMA.

Leine, R. I., D. H. Van Campen, and W. J. G. Keultjes. April, 2002. "Stick-Slip Whirl Interaction in Drillstring Dynamics." *Journal of Vibration and Acoustics* 209-220.

Liu, M, and D.G Gorman. 1994. "Formulation of Rayleigh damping and its extensions." *Computers & Structures* 277-285.

Logan, Daryl L. 2012. *A First Course in the Finite Element Method.* Stamford, CT, USA: Cengage Learning.

Macpherson, J. D., and J. S. Mason. 1993. "Surface Measurement and Analysis of Drillstring Vibrations." *SPE/IADC Drilling Conference.* Amsterdam, Netherlands: SPE/IADC.

Marquez, A., E. Omojuwa, and C. Teodoriu. 2017. "Mitigating Downhole Vibrations in Bottom Hole Assemblies Using Finite Element Analysis." *SPE Health, Safety, Security, Envieronment & Social Responsability Conference-North America.* New Orleans, Louisiana, USA: Society of Petroleum Engineers.

Melakhessou, H., A. Berlioz, and G. Ferraris. 2003. "A Nonlinear Well-Drillstring Interaction Model." *Journal of Vibration and Acoustics 125* 46-52.

Millheim, K., S. Jordan, and C. J. Ritter. 1978. "Bottom-Hole Assembly Analysis Using the Finite-Element Method." *SPE-AIME 51st Annual Fall Tehnical Conference and Exhibition.* New Orleans, LA: Society of Petroleum Engineers.

Moradi, S., and K. Ranjbar. 2009. "Experimental and computational failure analysis of drillstrings." *Engineering Failure Analysis* 923-933.

Navarro-Lopez, E. M., and D. Cortes. 2007. "Avoiding harmful oscillations in a drillstring through dynamical analysis." *Journal of Sound and Vibration* 151-171.

Omojuwa, E., S. Osisanya, and R. Ahmed. 2012. "Integrated Dynamic Analysis for Optimal Axial Load and Torque Transfer in BHAs Used for Extended-Reach Horizontal Wells." *SPE Eastern Regional Meeting.* Lexington, Kentucky, USA: Society of Petroleum Engineers.

—. 2011. "Measuring and Controlling Torsional Vibrations and Stick-Slip in a viscous-Damped Drillstring Model." *Internacional Petroleum Technology Conference.* Bangkok, Thailand: International Petroleum Technology Conference.

Patil, P. A. 2013. *Investigation of Torsional Vibrations in a Drillstring Using Modeling and Laboratory Experimentation (Doctoral Dissertation).* Clausthal University of Technology: Papierflieger-Verlag .

Patil, P. A., and C. Teodoriu. 2013. "Model Development of Torsional Drillstring and Invesigating Parametrically the Stick-Slips Influencing Factors." *Journal of Energy Resources Technology 135 (1)* 1-7.

Patil, Parimal Arjun, and Catalin Teodoriu. 2013. "A comparative review of modelling and controlling torsional vibrations and experimentation using laboratory setups." *Journal of Petroleum Science and Engineering* 227-238.

Pavone, D.R, and J.P. Desplans. 1994. "Application of High Sampling Rate Downhole Measurements for Analysis and Cure of Stick-Slip in Drilling." *SPE Annual Technical Conference and Exhibition.* New Orleans, Louisiana: SPE.

Rao, Singiresu S. 2007. *Vibration of Continuous Systems.* Hoboken, New Jersey: John Wiley & Sons, Inc.

Schmitz, Tony L., and Scott K. Smith. 2011. *Mechanical Vibrations Modelling and Measurement.* Springer.

Shor, R. J., M. Pryor, and E. Van Oort. 2014. "Drillstring Vibration Observation, Modeling and Prevention in the Oil and Gas Industry." *ASME 2014 Dynamic Systems and Control Conference.* San Antonio, TX: ASME.

Sotomayor, Gabriel P.G, Joao Carlos Placido, and J.C Cunha. 1997. "Drillstring Vibration: How to Identify and Suppress." *Fifth Latin American and Caribbean Petroleum Engineering Conference and Exhibition.* Rio de Janeiro, Brazil: Society of Petroleum Engineers, Inc.

Tucker, R. W, and C. Wang. 1999. "An Integrated Model for Drill-String Dynamics." *Journal of Sound and Vibration* 123-165.

Younggang, Liu, Li Fangpo, Xu Xin, Yang Biyu, and Lu Caihong. 2011. "Simulation Technology in Failure Analysis of Drill Pipe." *2011 SREE Conference on Engineering Modeling and Simulation.* Elsevier. 236-241.

Appendix A: Comparative Table of Experimental Research

Researcher (Year)	Investigation	Approach	Setup details	Main focus/Limitations
Melakhessou et al. (2003)	Study of nonlinear interaction between drillstring and wellbore with the help of model and experiment	Modeling with four DOF and experimental	Drillstring dia. 4 mm, wellbore dia. 24 mm, stabilizer dia. 20 mm, 180 RPM, 3 m in length with inertial disk located at the middle.	The study focuses on the BHA which is in compression. Only lateral vibrations investigated.
Mihajlovic et al. (2006)	Study of friction induced limit cyclcing in a flexible rotor system.	Modeling with two DOF and experimental	Drillstring length 1.47 m, added mass 0.45 kg	Observations made was that the normal force in the friction component can induce higher negative damping for higher normal forces giving rise to stick-slip
Raymond et al. (2008)	Defining best operational parameters to eliminate axial vibrations	Experimental	Drillstring length 3 ft, 3 in diam. PDC bit 3.5 in diam.	Experiment is limited to axial mode of vibration.
Khulief and Al-Sulaiman (2009)	Studied impact of drillstring with the wellbore. Model accounts torsional-bending and axial-bending nonlinear coupling	Modeling with Lagrange approach and experimental	Drillstring length 1-2 m, dia. 3-10 mm, 50-100 RPM	Sophisticated dynamic models need to be developed to investigate coupling modes of vibrations
Lu et al. (2009)	Reproduction of stick-slip vibration in laboratory for D-OSKILL mechanism	Experimental	Drillstring stiffness 0.6706 Nm/rad, 190 RPM, Nominal WOB 180 N. Length not provided	Smaller ROP with D-OSKILL mechanism due to loss of optimal WOB while effectively mitigating stick-slip vibrations.
Franca (2010)	To prove the drillstring response model on the basis of literature.	Experimental	10-400 RPM. ROP 0.01 mm/s to 100 mm/s. Bits 63.5 mm and 74.6 mm in length	Drilling rig has ability to provide ROP from 0.01-100 mm/s. The rock sample is driven instead of the drilling assembly.
Foster et al. (2010)	To reproduce lateral vibrations. Understand and quantify the behavior of AVDT.	Experimental	Drillstring length 2 m, dia. 5 mm, WOBs 1, 1.5 and 3.5 Kg, for torsional rig dia. 1 mm, wellbore dia. 8 mm, 400 RPM	Inertia wheels used to replicate the top drive and the BHA. Accelerometers used to measure shocks ocurring between the drillstring and borehole
Foster (2011)	To reproduce torsional vibrations. Understand and quantify the behavior of AVDT.	Experimental	Drillstring length 1.25 m, stiffness adjustable by varying tension, load 1-1.5 kg, Max WOB 20 N, 400 RPM	Axial excitation succesfully mitigated stick-slip.
Esmaeili et al. (2012)	Investigation of drillstring dynamics.	Experimental	Drillstring length 0.524 m, dia. 40 mm, 360 RPM, WOB 800 N.	Increasing WOB and rotary speed increases ROP. Keeping constant WOB and by reducing rotary speed, vibrations and ROP decreases
Patil (2013)	Investigation of drillstring dynamics	Modelling and Experimental	Drillstring length 5 m, drillstring OD 6 mm, drillstring ID 4 mm, 0-200 rpm, WOB 0 - 15 Kg, TOB 370.3 mNm, stiffness 0.02 Nm/rad	Only recreated the BHA of a drillstring.
Kovalyshen (2014)	Investigation of drillstring dynamics with drag bits.	Experimental	Bit dia. 49 mm, torsional stiffness 0.05-14 Nm/rad, 10-400 RPM. Only drill bit was used.	No drillstring was used, only a small shaft and a drill bit. Rock sample was used in the experiment.
Kapitaniak et al. (2015)	Investigation of drillstring dynamics.	Modelling and Experimental	Drillstring dia. 10 mm, 0.5-54 RPM, WOB 0.85-2.19 kN. Length not provided but assumed to be about 1 m	Limited in size. Finite Element Model used to calibrate setup. Calculated TOB from WOB and RPM.
Westermann et al. (2015)	Investigation of drillstring dynamics with the uniqueness of measuring side forces	Experimental	Drillstring length 5.4 m with 44.5 mm OD and 19.5 mm ID. Torque 107 Nm. 1,450 RPM max. WOB 14 kN max.	Focuses on studing lateral and torsional vibration. Measures side forces. Limited in size and no combination of types of vibration were provided.